Plant Physiology and Biochemistry 239 (2026) 111732

Contents lists available at ScienceDirect

Plant Physiology and Biochemistry

journal homepage: www.elsevier.com/locate/plaphy

Beyond stomata: a novel role of EPFL9-2 in regulating root system architecture and hydraulics in grapevine

Umar Shahbaz [a,b], Pierre Videau [c], Simon Josef Unterholzner [d], Ares Zanocco [a], Stefano Piazza [a], Paolo Sonego [a], Sara Ammanniti [b], Pier Luigi Bianchedi [a], Domenico Masuero [a], Massimo Pindo [a], Mickael Malnoy [a], Fabio Fiorani [e], Olivier Zekri [c], Michele Faralli [b], Lorenza Dalla Costa [a,*]

[a] Research and Innovation Centre, Fondazione Edmund Mach, San Michele all'Adige, Italy
[b] Center Agriculture Food Environment (C3A), University of Trento, San Michele all'Adige, 38098, Italy
[c] Novatech, Mercier Groupe, Le Champ des Noels, France
[d] Competence Centre for Plant Health, Free University of Bozen-Bolzano, Piazza Università, 1, Bolzano, 39100, Italy
[e] Institute of Bio- and Geo-Sciences, Forschungszentrum Jülich GmbH, Jülich, 52425, Germany

ARTICLE INFO

Keywords:
Epidermal patterning factor like 9
Stomagen
CRISPR/Cas9
Vitis spp.
Root system architecture
Lignin deposition
Xylems
Water stress
Climate change

ABSTRACT

Epidermal Patterning Factors (EPFs) are small plant peptides crucial for various physiological and developmental processes. While EPFL9 positively regulates leaf stomatal formation in crops, its function in other organs remains poorly understood. This study elucidates the role of *VviEPFL9*-2 in grapevine roots. Morphological and physiological traits were assessed in *epfl9*-2 knock-out (KO) lines of the rootstock 'Kober 5BB' under well-watered (WW) and water-stressed (WS) conditions, and in grafted plants with combinations of WT and KO scions and rootstocks. A multi-omics and immune-histological analysis of root tissues was also performed. KO root apparatus had a significant reduction in geotropic angle and total length, accompanied by an increase in root diameter and KO stems displayed more xylem vessels with a smaller section area. This phenotype persisted even when KO rootstocks were grafted with a WT scion. KO lines exhibited improved water-use efficiency under both WW and WS conditions. At the molecular level, edited roots showed strong activation of the lignin and salicylic acid pathways, confirmed by the confocal analysis of root tips and by the phytohormone profile. Our results demonstrate for the first time that *VviEPFL9*-2 loss-of-function induces profound root anatomical, morphological, and physiological modifications that are potentially beneficial for drought tolerance.

1. Introduction

In the context of climate change, a substantial investment is being directed towards the development of drought-resistant crop varieties (Vadez et al., 2024). In conditions of suboptimal water availability, plants minimize water loss and enhance soil water absorption via synchronized physiological and morphological adaptations (Feng et al., 2022; Kooyers, 2015; Uga et al., 2013). These responses are tissue-specific and influence the movement of water into plants from the soil to the atmosphere, primarily through roots, xylem vessels, and stomata (Fromm, 2019). The extent to which such organs can adapt to environmental conditions varies between and within species, resulting in a broad genotypic tolerance to drought (Mori and Inagaki, 2012; Guha et al., 2018). Studies on plant-water relations have concentrated on the above-ground traits due to the greater feasibility of their investigation (Lynch, 2019). However, roots play a critical role in responding to water stress by altering their hydraulic properties and architecture, namely with modifications in the length, branching, geotropic angle, and root thickness (Teng et al., 2023; Kou et al., 2022; Fromm, 2019). Although underexploited, improving root phenotypes to make crops

* Corresponding author.
E-mail addresses: umar.shahbaz@inrae.fr (U. Shahbaz), pierre.videau@mercier-groupe.com (P. Videau), simonjosef.unterholzner@unibz.it (S.J. Unterholzner), ares.zanocco@edu.unito.it (A. Zanocco), stefano.piazza@fmach.it (S. Piazza), paolo.sonego@fmach.it (P. Sonego), Sara.Ammanniti@laimburg.it (S. Ammanniti), pierluigi.bianchedi@fmach.it (P.L. Bianchedi), domenico.masuero@fmach.it (D. Masuero), massimo.pindo@fmach.it (M. Pindo), mickael.malnoy@fmach.it (M. Malnoy), f.fiorani@fz-juelich.de (F. Fiorani), olivierzekri@gmail.com (O. Zekri), michele.faralli@unitn.it (M. Faralli), lorenza.dallacosta@fmach.it (L. Dalla Costa).

https://doi.org/10.1016/j.plaphy.2026.111732
Received 26 June 2026; Received in revised form 31 August 2026; Accepted 7 September 2026
Available online 9 September 2026
0981-9428/© 2026 The Authors. Published by Elsevier Masson SAS. This is an open access article under the CC BY license (http://creativecommons.org/licenses/by/4.0/).

more adapted to the issues of modern agriculture is a very promising strategy (Schneider and Lynch, 2020). A recent study shows that the increased root plasticity improves crop stability under varying water conditions, emphasizing the importance of studying root architecture in stress tolerance (Zhao et al., 2025).

Several members of the Epidermal Patterning Factor family (EPF), which are well-characterized for their role in stomagenesis (Lin et al., 2017), have recently been linked to novel functions in non-foliar organs. For instance, Mohammed and colleagues (2019) hypothesized an involvement of EPF1 in root cortical aerenchyma formation in rice. In Arabidopsis, the peptides EPFL4 and EPFL6, secreted by the endodermis act as a ligand for the ERecta (ER) and ERECTA-LIKE 1 (ERL1) receptors in the phloem, a communication essential for the proper development of the procambium in inflorescence stems (Uchida and Tasaka, 2013). The ERecta-EPFs module coordinates the order of tissue layers (xylem, cambium, phloem) and the area of xylem vessels in *Arabidopsis* stems (Wang et al., 2019). Moreover, the heterologous expression of cotton genes *GhEPF2*-2 and *GhEPFL9*-6 in *Arabidopsis* significantly modifies primary root length and density compared to the WT under both normal and stress conditions (He et al., 2026). In addition, it has been found that members of the EPF/EPFL family are expressed in roots of different crops: *ZmEPF2*-1 and *ZmEPFL3* in maize (Xia et al., 2024), *PtEPFL1*-2, *PtEPFL5*-1, *PtEPFL5*-2, *PtEPFL8* in Populus (Liu et al., 2024) and *GhEPF19* and *GbEPF14* in cotton (Li et al., 2024).

EPFs are perceived by the ERECTA family (ER) receptor kinases but the specificity of the recognized EPFs peptide is dictated by the co-receptor TOO MANY MOUTHS (TMM) (Lin et al., 2017). It has also been shown that the components of the intracellular signaling cascade activated by the receptor complex ER-TMM are in common between different developmental processes like stomatal development (Bergmann et al., 2004) and floral organ differentiation (Bemis et al., 2013). Furthermore, mutants of YODA, a MAPK kinase involved in ER-TMM intracellular signaling, showed an impairment in the initiation of the embryonic primary root (Lukowitz et al., 2004), suggesting a specific role of the pathway regulated by EPF factors in determining root morphogenesis.

Grapevine (*Vitis* spp.) is one of the most economically important fruit trees, cultivated in over ninety countries mainly to produce wine, table grapes, raisins, distilled spirits and fruit juices (Atak, 2025). Many genomic, transcriptomic and physiological studies have been carried out in grapevine, to identify the genetic bases of traits of interest (Gambetta et al., 2020). This, combined with the fact that the most favorable environment for viticulture is a Mediterranean climate characterized by warm and dry summers, has made *Vitis* genus a model for studying the physiological processes of drought adaptation in perennial fruit trees (Gambetta et al., 2020). In grapevine, two paralogs of the *EPFL9* gene exist, named *VviEPFL9*-1 and *VviEPFL9*-2 (Clemens et al., 2022). It has been shown by our group that *VviEPFL9*-2 is the paralog that plays a major role in inducing stomatal formation. Moreover, we found that it is also expressed in roots and its expression is down-regulated in water-stressed genotypes (Shahbaz et al., 2025). In this study we investigated the biological function of *VviEPFL9-2* in root tissues, a role that remains largely unexplored. As a grapevine genotype we used 'Kober 5BB' (*Vitis berlandieri* x *Vitis riparia*), which is one of the most used rootstocks in Italian viticulture. Based on our recent findings (Shahbaz et al., 2025), we hypothesized that *VviEPFL9*-2 plays a functional role in root morpho-anatomy and systemic water-use efficiency (WUE). Specifically, we postulated that the loss-of-function of *VviEPFL9*-2 would induce adaptive alterations in root system architecture and vascular morphology, ultimately impacting whole-plant hydraulic responses under varying water regimes. Specifically, we aimed to address the following questions: (i) How does the *epfl9*-2 knockout affect root characteristics and plant physiology under well-water and water-stressed conditions? (ii) Are those characteristics maintained when *epfl9*-2 edited rootstock is grafted with wild-type scions? (iii) Which are the genes and metabolic pathways modulated by the *VviEPFL9*-2 knockout in roots?

2. Materials and methods

2.1. Gene expression analysis of VviEPFL9-2 in roots of a panel of rootstocks

A set of in vitro-cultivated rootstocks was analyzed for their expression of *VviEPFL9*-2 in roots. These genotypes derive from the cross of different *Vitis* species: Kober 5BB and SO4 belong to the *Vitis berlandieri* x *Vitis riparia* group; 1103 Paulsen and 110 Richter belong to the *Vitis berlandieri* x *Vitis rupestris* group, 101.14 and Schwarzmann belong to the *Vitis riparia* x *Vitis rupestris* group and Georgikon derives from the hybridization between the rootstock Kober 5BB and a *Vitis vinifera* genotype. Total RNA was extracted from roots of plants cultivated in vitro for 50 days. After collection, roots were immediately frozen in liquid nitrogen. The protocol used to extract RNA and to quantify *VviEPFL9*-2 expression is described in Shahbaz et al. (2025). For each biological replicate of each genotype, two technical replicates were run on a single plate. The real-time PCR runs were carried out using the LightCycler® 480 Instrument II (Roche Diagnostics, Rotkreuz, Switzerland) and data were analyzed using the LightCycler® 480 software II (Roche Diagnostics, Rotkreuz, Switzerland).

2.2. Edited plant material

Gene transfer experiments were carried out and described in Shahbaz et al. (2025) (two binary vectors were used each with a specific guide RNA to target a different region of the third exon of *VviEPFL9*-2 (Vitvi05_01chr07g18680): (1) sgRNA_937 CATTCATTGTAAGTGCAGGT (reverse strand) and (2) sgRNA_938 GACTGATGATTGGATCCACC (forward strand). Regenerated plants were screened by PCR for the presence of SpCas9 and subsequently analyzed by Illumina amplicon sequencing for the analysis of the mutation profile in the target site. Both procedures were described in Shahbaz et al. (2025). The methods used for the analysis of the T-DNA integration copy number and the identification of the T-DNA integration point are described in Dalla Costa et al. (2021). The binary vectors used for transformation were designed to include a T-DNA excision system. This consisted in the FLP recombinase, under the control of a heat-shock inducible promoter (Dalla Costa et al., 2016) and FRT recombinase recognition sites next to the left and right borders (Fig. S2c). Propagated buds of Kob_*epfl9*-2a and Kob_*epfl9*-2b were incubated four times at 43°C for 6-h with at least 48-h interval between consecutive incubations in a hybridization oven 'hybridizer HB-1000' (UVP, Upland, CA). After 1 month from the last incubation, two leaves of the shoots grown from the induced buds were collected for DNA extraction and SpCas9 quantification, according to the copy number method detailed in Shahbaz et al. (2025). To further check the removal of the T-DNA cassette in these biological replicates, a qualitative PCR was carried out in 20 μl final volume containing 1×PCR BIO (Resnova, Rome, Italy), 0.5 μM of each primer (these primers anneal to regions close to LB and RB; Fw_LB: TGTAGATGTCCGCAGCGTTA; Rv_RB: TGATCGGGTACCTGAAGTTCCT, Fig. S2c) and 20 ng of genomic DNA. The amplification fragment (238 bp) was sequenced using the Sanger method.

2.3. Water stress experiment on edited rootstock

Plant material. Ten biological replicates of Kob_WT and mutant Kob_*epfl9-2a* and Kob_*epfl9*-2b were acclimatized in the greenhouse in 0.25 L plastic pots with holes in the bottom to allow for water drainage, filled with the substrate Extra quality-Semina 80 (TerComposti, Calvisano, Italy) and covered by parafilm on the top. According to technical specifications, the volumetric water content of Extra quality-Semina 80 substate at container capacity (pF1 = −10 hPa) is 70% (v/v). Plants were grown in a growth chamber (PPFD 100 ± 20 μmol m^{-2} s^{-1}, 24°C,

16/8 light/dark photoperiod). After 7 days, the parafilm was initially opened by creating small slits and then completely removed. After 15 days, plants were potted into rhizotrons.

Rhizotron construction. The rhizotrons (Fig. S3 and Fig. S6) were custom-built in our laboratory using an aluminum frame. One side featured a transparent polymethyl methacrylate (PMMA) sheet (2 mm) to facilitate root imaging, while the rear panel was opaque black to block light transmission. To ensure roots were maintained in darkness during the growth period, the transparent face was covered with a removable black plastic shield when imaging was not in progress. Each rhizotron measured 50 cm in height, 25 cm in width, with an internal depth of 4.7 cm. Two drainage holes were positioned at the bottom to prevent waterlogging. The weight of each empty rhizotron was approximately 1.5 kg.

Transplantation in rhizotrons. Before planting, the rhizotrons were opened and carefully filled with approximately 1900 g of fine soil (Extra quality-Semina 80, TerComposti, Calvisano, Italy), which was compacted by gently pressing down from the top. Plants were carefully removed from the 0.25 mL plastic pots and were then gently placed at the center of the rhizotron. The total weight of the rhizotron, soil, and plants was brought to 3600 g and after a manual irrigation to 4100 g (around field capacity). Considering an empty container weight of approx. 1500 g, the net mass of substrate, plant, and water was about 2600 g, representing an initial water volume of approx. 1500 g. Rhizotrons were covered with aluminum foil and arranged in a fully randomized manner to minimize positional effects.

Experimental design. Rhizotrons were arranged in two equal blocks (large benches) of a GMO greenhouse. Plants were exposed to natural light supplemented, when needed, with high-pressure sodium lamps providing a PPFD of 200-250 μmol m^{-2} s^{-1}. The photoperiod was 16/8 h (light/dark) and the temperature was maintained between 18°C and 22°C. After 10 days of acclimatation, water stress was imposed on half of the biological replicates (n = 5) of the WT and mutant lines (water stressed plants) by withholding the water for a period of 28 days while the other half (well-watered plants) were manually irrigated daily after a gravimetric measurement to maintain target rhizotron weight at 4100 g. Following the water stress experiment, whole root systems were removed from rhizotrons and thoroughly washed with distilled water. To minimize RNA and metabolite degradation, each cleaned root sample was immediately snap-frozen in liquid nitrogen and subsequently stored at −80°C. Prior to transcriptomic and metabolomic analysis, frozen samples were ground to a fine powder using an IKA A11 analytical mill (IKA-Werke GmbH & Co, Staufen, Germany).

Stomatal density (SD) and stomatal size (SS) measurements. The methods used were described in Shahbaz et al. (2025). For each plant a leaf was analyzed (the 5th from the apex). For each leaf three imprints were taken, and for each imprint, three different images were acquired. ImageJ software (https://imagej.nih.gov/ij/) (Schneider et al., 2012) was used for image analysis, stomatal counting and stomatal pore length. Stomatal density was quantified using the "Multi-point" tool to manually tag and count individual stomata within a defined region of interest (ROI) calibrated in millimeters. For stomatal pore length, the "Straight Line" tool was used to measure the maximum longitudinal axis of the pore aperture. Pixels were converted to micrometers using the "Set Scale" function, calibrated against a stage micrometer captured under the same magnification. No automated plugins were employed. From each image, eight randomly selected stomata were measured.

Root morphological measurements. Root system images were acquired non-destructively on a weekly basis for four consecutive weeks (specifically on days 3, 11, 18, and 25 following the onset of water stress). Images were captured using a Canon EOS 40D camera positioned in front of the transparent rhizotron interface. To ensure reproducibility, camera angle, distance, and lighting conditions were strictly standardized across all sessions. In parallel with imaging, root morphological traits were measured manually in situ through the transparent rhizotron panel. Root length was measured using a graduated metal rule (resolution: 1 mm) aligned against the transparent surface. Root diameter was assessed using a professional digital caliper (SCU, Germany; precision 0.01 mm) placed directly on the external face of the panel corresponding to the root position. The three thickest primary roots per plant, selected according to a visual inspection of the entire root system in the rhizotron, were measured and averaged. Root Spreading Angle (RSA) was quantified with ImageJ software (https://imagej.nih.gov/ij/) on images captured at the end of the experiment using the Angle Tool. For each plant, a vertical reference line was drawn from the root-shoot junction to represent the vertical axis. The spreading angle of each root was then measured as the deviation from this vertical reference line. When multiple roots were present, the same reference point was used consistently to ensure comparable measurements across samples. To analyze root distribution at different depths, the rhizotron profile was divided into four distinct horizontal zones, labeled A (superficial) through D (deep). Within each zone, RSA was calculated as the deviation from the vertical axis, following the method described by Lesmes-Vesga et al. (2023).

Gas-Exchange measurements. Gas-exchange parameters, specifically CO_2 assimilation rate at saturating PPFD (A_{sat}), stomatal conductance (g_s) and intrinsic water-use efficiency ($_iWUE$) calculated as A_{sat}/g_s were measured using a portable infrared gas analyzer (LI-6400, LI-COR Biosciences Inc., Lincoln, NE, USA). Measurements were performed with a 2 cm^2 leaf cuvette equipped with an integrated blue-red LED source. Inside the cuvette, environmental conditions were maintained at a flow rate of 400 μmol s^{-1}, a leaf temperature of 25°C, and a light intensity at 1000 PPFD (μmol m^{-2} s^{-1}). External CO_2 was set at 420 ppm, with VPD and relative humidity kept at 1.5 kPa and 50 ± 10%, respectively. Data were collected at 2, 7, 10, 14, 17, 21, 23, and 28 days after stress application (DASA).

2.4. Grafted plant experiment

Plant material. For the scion, a shoot tip (apical meristem and a part of stem) or a nodal explant was taken from 2-month-old 'Syrah' plants (5-6 cm tall) propagated in vitro in baby jars. For the rootstock, 2-month-old in vitro 'Kober 5BB' plants were cut at 1–1.5 cm from the base, using a sterile blade, excluding the first node. A vertical slit was made on the rootstock stem, into which the scion explant was inserted. Four distinct groups of grafted plants were produced, using a wild-type (WT) and an edited line (KO) for both the genotypes 'Syrah' (Sy) and 'Kober 5BB' (Kob): (i) Sy-KO_Kob-KO, (ii) Sy-KO_Kob-WT, (iii) Sy-WT_Kob-KO and (iv) Sy-WT_Kob-WT. A total of 10 micrografts were made for each group. Each graft was kept in sterile baby jars in WP medium (McCown and Lloyd, 1981) and grown in a climatic chamber (PPFD 100 ± 20 μmol m^{-2} s^{-1}, 24°C, 16/8 light/dark photoperiod). After 60 days from micrografting, the 5 healthy grafted plants for each group (a total of 20 grafted plants) were potted in 0.25 L plastic pots with three holes in the base to allow for water drainage. The pots were filled with a similar quantity of growing substrate Extra quality Semina 80 (TerComposti, Calvisano, Italy) and were covered with parafilm. The plants were maintained in a growth chamber (PPFD 100 ± 20 μmol m^{-2} s^{-1}, 24°C, 16/8 light/dark photoperiod) and holes were gradually made in the parafilm over the course of three weeks. Following a 23-day period, the plants were potted into rhizotrons.

Experimental design. The 20 plants were manually irrigated daily following a gravimetric measurement to maintain the rhizotron weight at 4100 g. The phenotyping period lasted 28 days. Of the 5 replicates of Sy-KO_Kob-WT only two survived and were phenotyped. Imaging sessions were conducted once a week for three consecutive weeks (on days 4, 11 and 17 from the start of the phenotyping period) using the same procedure as for the water stress experiment for root morphological measurements. Similarly, stomatal conductance and photosynthesis were measured four times (on days 10, 14, 17 and 23 from the start of the phenotyping period) using the portable infra-red gas analyser (LiCOR 6400-40XT). Lastly, total leaf area values were recorded at three

time-points (on days 1, 11 and 23 from the start of the phenotyping period) and were calculated as the sum of the areas of all the leaves of a plant, in turn calculated from the length of the leaf central vein. At the end of the experiment, four types of samples were separately collected for each grafted plant: (i) leaves, (ii) stems and petioles, (iii) roots (before sampling, roots were washed to completely remove soil and dried with hand paper), (iv) the piece of stem containing the grafting point. For the first three samples, fresh and dry weight (after 48 h in a stove at 80°C), were measured. Sample (iv) was immediately stored at –20°C to be used for xylem analysis.

2.5. Stems sectioning and xylem characterization

To analyze xylem morphology and vessel distribution, transverse cross-sections were obtained from both rootstock and scion stems. Stem segments (3–4 mm in length) were harvested using a razor blade immediately above the graft union (scion) and below the graft union (rootstock). Samples were mounted on cryostat chucks using PBS buffer as a freezing medium. The buffer was applied within the cryostat chamber to induce rapid freezing and form a supporting ice block. Sectioning was performed at −20°C using a Leica CM 1510 cryostat (Leica Microsystems, Nussloch, Germany). For each sample, 4–5 serial sections (45 μm thick) were collected, mounted on glass slides, and analyzed using a Nikon Eclipse E600W microscope (Nikon Corp., Tokyo, Japan) equipped with phase contrast optics and a high-resolution digital camera DS-Fi1 (Nikon Corp., Tokyo, Japan). Observations and images were acquired using a 4× objective with a numerical aperture of 0.10 (total visual magnification: 40X). Afterward, photos were analyzed using ImageJ software. A portion of the section was selected, using the "polygon selections" tool, and measured to have an area of 1 mm^2. In the selected area, xylem vessels were counted using the "multi-point" tool and their number was divided by the area obtaining xylem vessels density values ($\rho_{vessels}$). Xylem vessels dimensions were also measured; in particular, 25 xylem vessels were randomly selected and, using the "freehand selection" tool, the major and minor diameter of the vessel were measured as the maximum and minimum Feret's diameters of the selection. Also, the whole area of the section was measured. Ultimately, xylem vessel area ($A_{vessels}$) and theoretical hydraulic conductivity (k_h) were calculated using the following formulas: (i) $A_{vessel} = \pi . \left(\frac{d_{max}}{2}\right) . \left(\frac{d_{min}}{2}\right)$ where d_{max} is the major diameter of the vessel, and d_{min} is the minor diameter of the vessel; (ii) $k_h = \frac{\pi \rho}{128 \eta} \cdot \left(\frac{d_{Max} + d_{min}}{2}\right)^4 . N_{vessels}$ where ρ is the fluid density (assumed to be 1000 kg m^{-3}), η is the viscosity (assumed to be 1×10^{-9} MPa/s) and $N_{vessels}$ is the number of vessels in the section calculated as $N_{vessels} = \rho_{vessels} . A_{Section}$. This formula was obtained according to the modified Hagen-Poiseuille law described by Tyree and Ewers (1991).

2.6. Transcriptomics analysis

RNA extraction and RNA sequencing. Total RNA was extracted from finely powdered root samples of 3 biological replicates of Kob_WT and mutants Kob_*epfl9-2a* and Kob_*epfl9*-2b kept in well-watered conditions, using the Spectrum Plant Total RNA Kit (Sigma–Aldrich, St. Louis, MO, USA), and following the manufacturer's protocol. After DNase treatment, RNA was precipitated using 0.1 vol of sodium acetate 3M and 3 vol of cold ethanol. 1.5 μg of high-quality RNA was used for library preparation and sequencing. Paired-end reads of 150 bp long sequences were obtained for each of the 9 samples using the Illumina NovaSeq 6000 sequencing platform. Approximately 50 million strand-specific sequences were obtained for each sample. The quality of the raw data was checked using FastQC (version 0.11.9) (Leggett et al., 2013) and the reads were preprocessed for both adapter clipping and quality trimming with fastp (version 0.23.2) (Chen et al., 2018). The resulting pre-processed reads were aligned to the reference genome of *Vitis vinifera* T2T.v5 (Shi et al., 2023) using the hisat2 aligner (version 2.2.1) (Kim et al., 2019) and raw read counts were extracted using the featureCount read summarization program (version 1.6.4) (Liao et al., 2014) based on the v.4.3 annotation (downloaded from Grapedia, https://grapedia.org/files-download/). All raw RNA-Seq read data are deposited in the NCBI Short Read Archive (http://www.ncbi.nlm.nih.gov/sra/) under the BioProject accession code PRJNA1256299. The differential expression analysis was performed via the limma's empirical Bayes procedure (version 3.40.2) (Ritchie et al., 2015) using the limma-trend method (Law et al., 2014). For each pair-wise comparison (Kob_*epfl9-2a* vs WT and Kob_*epfl9-2b* vs WT) genes with an FDR-adjusted p-values below 0.05 and a fold change above 2 were considered differentially expressed (DEG).

Over-representation and gene set enrichment analyses. Functional annotation of differentially expressed genes was performed using ShinyGO v0.82 (Ge et al., 2020) for Gene Ontology (GO) terms with standard settings (FDR < 0.05 and P-value < 0.05). Gene set enrichment analysis (GSEA) was performed on custom gene sets representing selected biological pathways and gene families using the fgsea R package (Korotkevich et al., 2021). Genes were ranked by signed -log10 (p-value) × log fold change (log2FC) from differential expression analysis: the more significant a gene is differentially expressed, the larger that value will be. Enriched pathways were considered significant at an FDR-adjusted p-value below 0.05.

Rank-Rank Hypergeometric Overlap (RRHO) Analysis. In addition to standard differential expression analyses, a Rank–Rank Hypergeometric Overlap was applied (Plaisier et al., 2010) using the RRHO2 (v1.0) package (Cahill et al., 2018) to compare transcriptomic signatures of our two edited rootstock lines relative to the wild-type. RRHO is a threshold-free, agnostic approach which ranks two gene lists by their p-value and effect size direction and assesses the statistical significance of gene overlapping across all rank cutoffs. The RRHO analysis performed on the ranked lists by signed -log10(padj) for both Kob_ epfl9-2a vs WT and Kob_ epfl9-2b vs WT returned as output an heatmap features four quadrants: upper-right (genes concordantly up-regulated in both edits), lower-left (genes concordantly down-regulated), and the two discordant quadrants (up in one edit but down in the other).

2.7. Histochemical analysis

Histochemical staining of cell wall components in root tips was performed according to Ursache et al. (2018). Briefly, root tips from 45-day-old in vitro plants were fixed in 4% paraformaldehyde and cleared in ClearSee solution (Kurihara et al., 2015) for 3 weeks, with the solution exchanged every two days. Subsequently, samples were stained in ClearSee containing 0.5% Auramine-O for 24 h, followed by two washes in ClearSee (30 min and 60 min). Root tips were then counterstained in ClearSee containing 0.1% Direct Red 23 for 2 h and washed again in ClearSee (30 min and 60 min) before mounting on microscopy slides. Imaging was performed using a Zeiss LSM 800 confocal laser scanning microscope (Carl Zeiss, Jena, Germany). Auramine-O was excited with a 488 nm laser (emission collected at 505–530 nm), while Direct Red 23 was excited at 561 nm (emission collected at 580–615 nm).

2.8. Statistical analysis

Statistical analyses were performed using R software (R Core Team, 2020). A two-way ANOVA was used to evaluate differences between groups and *post hoc* comparisons using Tukey test were carried out to assess statistical significance among groups (*P* values lower than 0.05).

3. Results

3.1. VviEPFL9-2 knock-out in rootstocks influence above ground and underground morphological traits under different water availability

To functionally identify the role of *VviEPFL9*-2 in roots, we utilized *epfl9*-2 mutant 'Kober 5BB' lines generated by Shahbaz et al. (2025). The 'Kober 5BB' rootstock (*Vitis berlandieri* x *Vitis riparia*) was selected for functional analysis based on an initial evaluation of *VviEPFL9*-2 expression across a panel of rootstocks differing in morpho-physiological traits and soil drought tolerance. *VviEPFL9*-2 transcript levels were highest in 'SO4' and 'Kober 5BB', followed by the '1103 Paulsen', '110 Richter' and 'Georgikon 28' (Fig. S1). From the population of edited 'Kober 5BB' plants (Table S1), two independent edited lines were selected for phenotyping, Kob_*epfl9*-2a, and Kob_*epfl9*-2b. The Illumina sequencing of the target site revealed a complex mutation profile for the Kob_*epfl9*-2a line (the proportion between loss-of-function mutations and unaltered wt allele is 80%: 20%) while a homozygous loss-of-function mutation was found for the Kob_*epfl9*-2b mutant (i.e. a T insertion). The identification of a different T-DNA genomic integration point for the two lines, in both cases intergenic (Fig. S2a and b), demonstrated that they originated from independent genetic transformation events. The binary vector used to generate the edited lines was designed with the *Flp*/FRT site-specific recombination system (Fig. S2c) for the heat-shock inducible removal of the T-DNA to enhance societal acceptability and regulatory compliance. To test the feasibility of the T-DNA excision, dedicated in vitro biological replicates of Kob_*epfl9*-2a and Kob_*epfl9*-2b were subjected to heat treatment, while plants used for primary experimental assays were immediately acclimatized in the greenhouse without T-DNA removal. The excision mechanism was shown to be functional, although complete T-DNA excision was achieved in only one biological replicate per line (Fig. S2d and e).

Root system architecture was analyzed in rhizotrons under both well-watered (WW) and water stressed (WS) conditions. Initially, we confirmed the distinct stomatal patterning in the mutant lines compared to the WT. As shown in Fig. 1a and Fig. S3, stomatal density (SD) in mature leaves was significantly lower in the mutant lines compared to the WT. Mean SD values were 24 mm^{-2} for Kob_*epfl9*-2a and 11 mm^{-2} for Kob_*epfl9*-2b, representing reductions of approximately 78% and

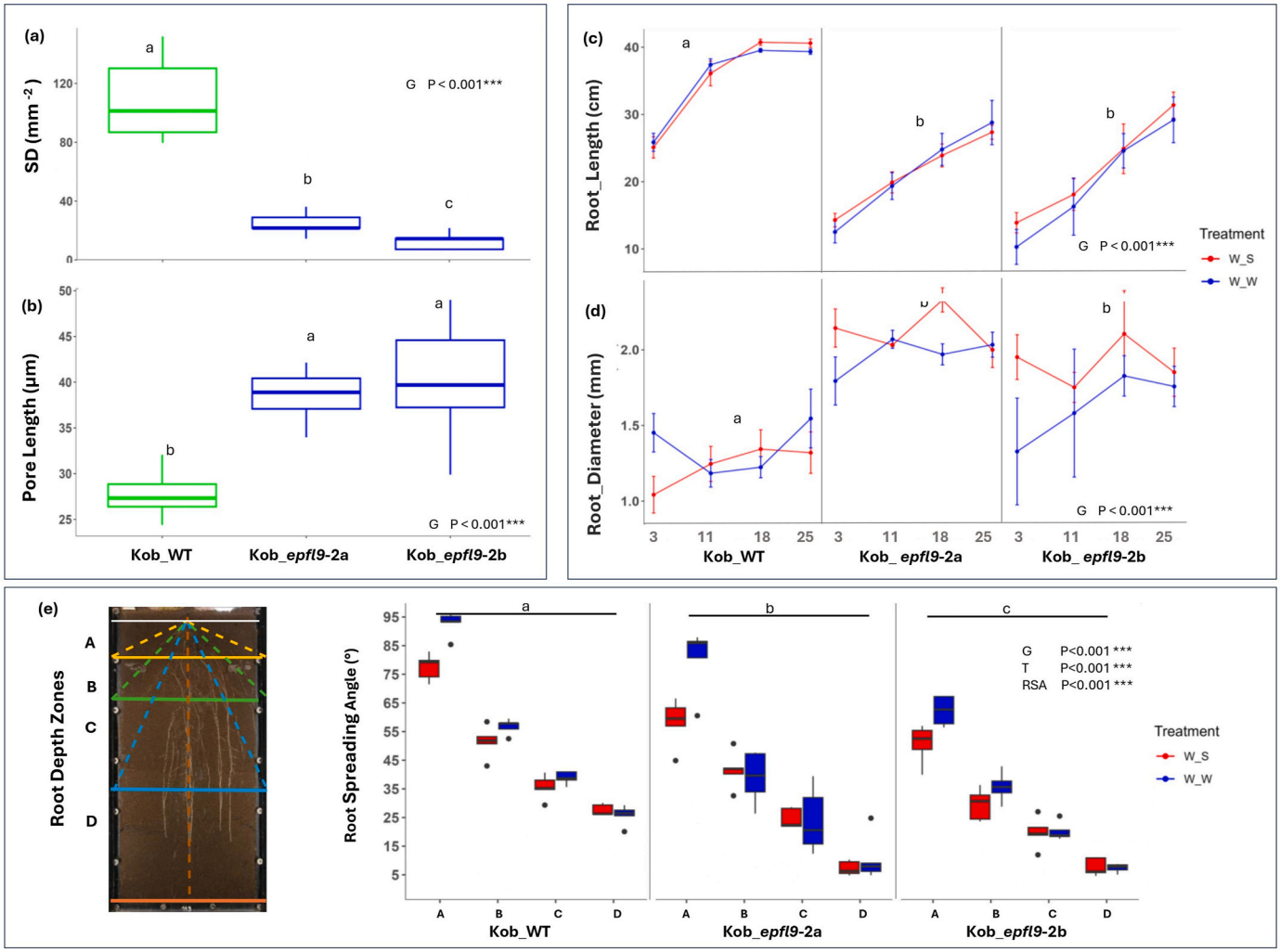


Fig. 1. Effects of *VviEPFL9*-2 knockout on above (leaf) and below ground (root) traits in 'Kober 5BB' *epfl9*-2 mutants and WT grown in rhizotrons under well-watered (WW) and water stress (WS) conditions. **(a)** Stomatal density (SD mm^{-2}) and **(b)** stomatal pore length (µm) measured in mature leaves (the 5th from the apex) of Kob_WT, Kob_*epfl9*-2a, and Kob_*epfl9*-2b plants. **(c)** Root length (cm) and **(d)** root diameter (mm) of each genotype under well-watered (WW, blue) and water stress (WS, red) conditions, measured at multiple time points. **(e)** (Left) Representative rhizotron image illustrating the segmentation into four depth zones (A–D) used for Root Spreading Angle (RSA) quantification. (Right panel) Mean RSA (°) measured in each depth zone (A–D) for Kob_WT and mutant lines under WW and WS conditions. Data represents means ± SE (n = 5). Significant differences (P < 0.05) are denoted by different letters, according to ANOVA and subsequent post-hoc analysis.

90% respectively, compared to the WT (109 mm^{-2}). Conversely, average stomatal pore length (Fig. 1b) increased in the edited lines (40.4 μm for Kob_*epfl9*-2a and 44.6 μm for Kob_*epfl9*-2b) compared to the WT (28.9 μm). Regarding below-ground traits, significant genotypic differences were observed for all measured root traits. Total root length was significantly lower in mutant lines compared to Kob_WT ($P < 0.001$) throughout the experiment, with no significant effect observed for the water treatment ($P = 0.62$; Fig. 1c). In terms of root thickness, mutant lines developed significantly thicker roots compared to the WT ($P < 0.001$; Fig. 1d): mean root diameter was 2.04 ± 0.05 mm for Kob_*epfl9*-2a and 1.79 ± 0.05 mm for Kob_*epfl9*-2b, versus 1.29 ± 0.05 mm for Kob_WT. Water treatment did not significantly influence diameter ($P = 0.10$). Root spreading angle (RSA) was quantified at four distinct soil depths (Zones A to D) (Fig. 1e). In the most superficial layer (Zone A), Kob_WT roots displayed the widest RSA, indicating a predominantly horizontal growth habit. In contrast, both mutant lines exhibited significantly narrower angles in the same zone, reflecting a steeper, more vertical root development. In deeper layers (Zones B, C, and D), RSA consistently decreased across all genotypes, with the sharpest reduction observed in Kob_*epfl9*-2b. Statistical analysis confirmed significant main effects for genotype, treatment, and depth zone ($P < 0.001$ for all variables).

3.2. *VviEPFL9-2 knock-out in rootstocks improve water saving behavior under water stress*

As shown in Fig. 2a, the CO_2 assimilation rate (A_{sat}) was consistently higher in WW plants compared to WS plants. Water stress induced a significant decline in A_{sat} across all genotypes, but the timing of this response varied: Kob_WT and Kob_*epfl9*-2a experienced a fast drop in assimilation rate while Kob_*epfl9*-2b maintained it comparable to WW controls until 15 days after stress application (DASA). At 21 DASA,

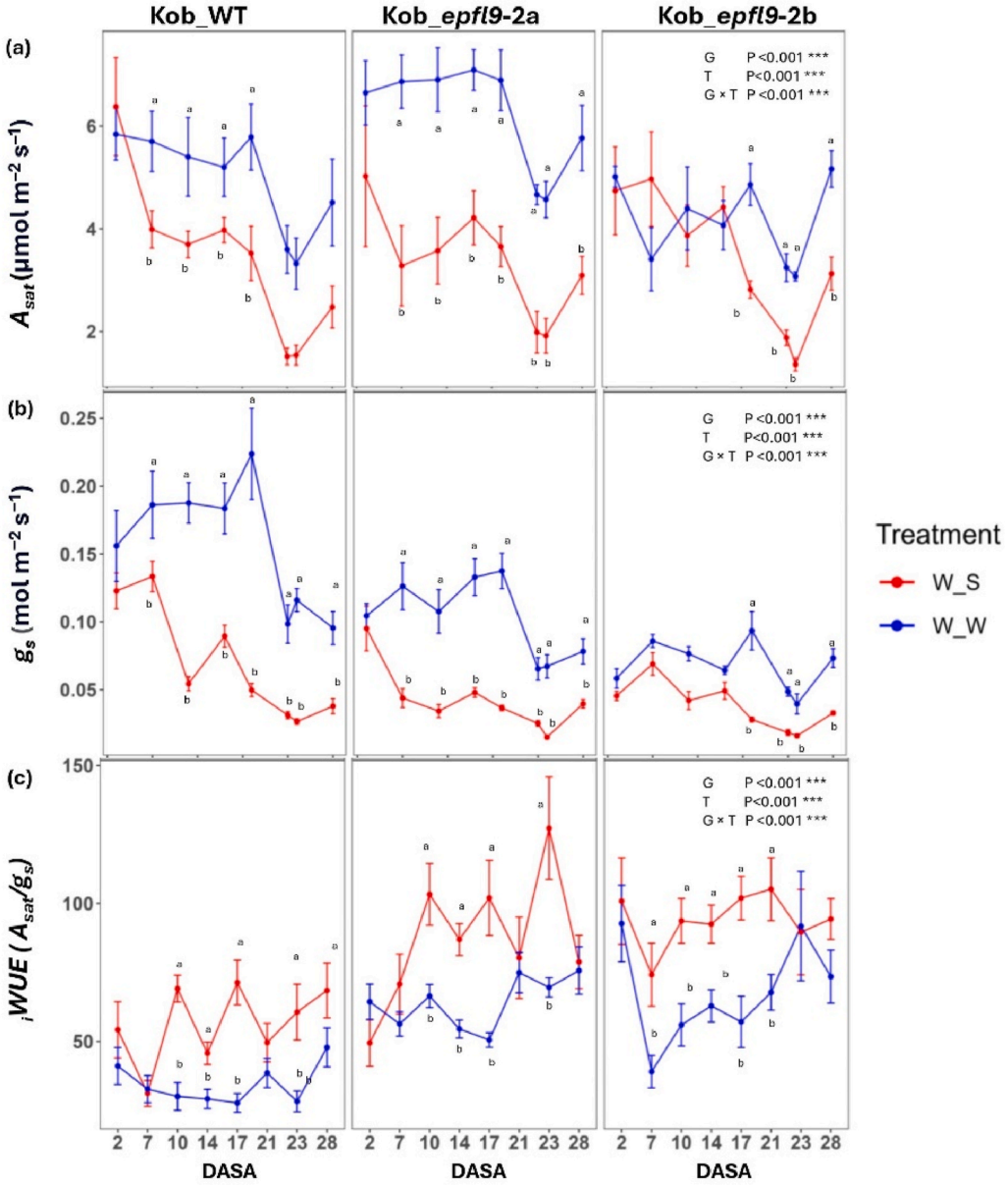


Fig. 2. Photosynthetic traits in 'kober 5BB' *epfl9*-2 mutants and WT under well-watered (WW) and water stress (WS) conditions. **(a)** CO_2 assimilation rate at saturating light (A_{sat}), **(b)** stomatal conductance (g_s), and **(c)** intrinsic water-use efficiency ($_iWUE$) calculated as A_{sat}/g_s over a 25-days period under WW (blue line) and WS (red line) conditions. Measurements were taken at multiple time points expressed as Days After Stress Application (DASA). Data represent means ± SE ($n = 5$). Significant differences ($P < 0.05$) are denoted by different letters, according to ANOVA and subsequent Tukey's post-hoc analysis.

Kob_WT plants showed a substantial decrease in A_{sat}, from approximately 6.4 to 1.5 μmol m^{-2} s^{-1}. During the same period, A_{sat} declined from ~5.0 to 1.9 μmol m^{-2} s^{-1} in Kob_*epfl9*-2a and from ~4.7 to 1.3 μmol m^{-2} s^{-1} in Kob_*epfl9*-2b. Two-way ANOVA confirmed significant main effects for genotype (G), treatment (T), and their interaction (G×T) ($P < 0.001$). Differences in stomatal conductance (g_s) were even more pronounced than those for A_{sat} (Fig. 2b). Under WW conditions, both edited lines exhibited significantly lower g_s compared to the WT. However, under water stress, g_s values converged, becoming comparable between WT and mutant lines. Similar to photosynthesis, significant divergence in g_s between water treatments in Kob_*epfl9*-2b was observed only after 15 DASA. The significant G×T interaction ($P < 0.001$) reflects the fact that WT experienced a drastic reduction in g_s under stress, whereas the mutants showed a more moderate decline due to their constitutively lower conductance.

Intrinsic water use efficiency ($_i$*WUE*) (A_{sat}/g_s; Fig. 2c) was significantly higher in both mutant lines compared to WT irrespective of the water regime. Kob_*epfl9*-2b, exhibited a gain in $_i$*WUE* in WS conditions as early as 7 DASA. Statistical analysis demonstrated significant effects of genotype (G), treatment (T), and their interaction (G × T). Rhizotrons containing WT plants reached a final mean weight of 3138 g, corresponding to a cumulative water loss of approximately 960 g, more than 60% of total initial water content. This means that WT plants completely exhausted both the easily available water (EAW) and water reserve (WR) pools early in the experiment, spending the second half of the trial under severe matric stress (Fig. S4). Edited lines Kob_*epfl9*_2a and Kob_*epfl9*_2b, in contrast, maintained final weights of respectively 3442 g and 3475 g representing a cumulative loss of 658 g and 625 g (~33% water savings compared to WT) (Fig. S4). These plants preserved a significantly higher residual water fraction, delaying entry into matric stress. Regarding biomass accumulation at the end of the experiment, Kob_WT plants produced significantly higher leaf and stem dry mass compared to Kob_*epfl9*-2a and Kob_*epfl9*-2b under WW conditions ($P < 0.001$). Under WS, these differences were less pronounced albeit still significant (Fig. S5a and b).

3.3. The root phenotype of epfl9-2 mutants is maintained upon grafting with a wild-type scion

A grafting experiment was conducted to ascertain whether the distinctive root phenotype of the edited rootstock is a direct consequence of the mutation in root tissues or whether it is a secondary effect driven by the altered stomatal density of the scion. Four distinct groups of grafted plants were produced, using a WT and an edited line (KO) of 'Syrah' (Sy) as the scion and 'Kober 5BB' (Kob) as the rootstock. Given the availability of *epfl9*-2 edited 'Syrah' (the molecular characterization of the 'Syrah' edited line is available in Spinella et al., 2025) that is an internationally recognized and widely cultivated wine variety, we opted to use it as the scion for grafting experiments rather than 'Kober 5BB' which is exclusively utilized as a rootstock. This approach allowed us to simulate a realistic scion–rootstock combination. For the Sy-KO_Kob-WT combination only 2 biological replicates survived, therefore, the results for this grafting group are only indicative. As expected, the mature leaves of Sy-WT had a significantly higher SD than Sy-KO ($P < 0.001$), regardless of the rootstock used (Fig. 3a). The approximate mean SD was 137 mm^{-2} and 120 mm^{-2} for Sy-WT grafted onto Kob-WT or Kob-KO respectively, and 29 mm^{-2} and 20 mm^{-2} for Sy-KO grafted onto Kob-WT or Kob-KO respectively (Fig. 3a). Conversely, stomatal pore length was significantly greater in Sy-KO scions compared to Sy-WT (Fig. 3b). Root length showed significant differences among the grafted combinations (Fig. 3c) ($P < 0.001$). After 30 days, the roots of Sy-KO_Kob-WT and Sy-WT_Kob-WT reached the bottom of the rhizotrons (40 cm) while those of Sy-KO_Kob-KO and Sy-WT_Kob-KO showed shorter mean length values (23.2 ± 2.46 and 27.0 ± 3.76, respectively) ($P < 0.001$) (Fig. 3c). Regarding root diameter, Kober KO showed higher values compared to Kober WT, independently from the grafted scion: 1.6 ± 0.06 mm and 1.4 ± 0.05 mm in Kober KO grafted with Sy-WT or Sy-KO scion, respectively, and 0.58 ± 0.14 and 1.08 ± 0.05 in Kober WT grafted with Sy-WT or Sy-KO scions (Fig. 3d). In contrast to root morphology, root biomass accumulation appeared to be influenced by the scion genotype (Fig. 3e and f). Root fresh and dry weights were significantly higher in plants grafted with a Sy-WT scion compared to those with a Sy-KO scion. However, regarding the Sy-KO/Kob-WT combination, it must be noted that only two of the five initial replicates survived, and these plants exhibited severe growth retardation, preventing robust statistical assessment for this specific group. Root spreading angles analyzed at the end of the phenotyping revealed significant variation among the four groups. In zone A and D, Sy-WT_Kob-WT roots show the widest root spreading angle, significantly greater than Sy-KO_Kob-KO ($P < 0.05$) while depth zones B and C showed no significant variations (Fig. 3g). The Sy-KO_Kob-WT group was not analyzed due to the limited number of viable biological replicates and to the few visible roots in the rhizotrons. Overall, these results indicate that the short, thick, and steep root phenotype of the *epfl9*-2 mutant is not rescued by grafting with a WT scion. These features can be visualized in Fig. S6.

3.4. The epfl9-2 edited rootstock influences physiological and structural parameters of grafted WT scion

Leaf gas exchange measurements were conducted on grafted combinations to determine whether the *VviEPFL9*-2 mutation in the rootstock influences photosynthetic rate and stomatal conductance in the scion. As shown in Fig. 4a, Sy-WT_Kob-WT and Sy-WT_Kob-KO exhibited significantly higher CO_2 assimilation rates (A_{sat}) (7.11 ± 0.44 μmol $m^{-2}s^{-1}$ and 7.62 ± 0.39 μmol $m^{-2}s^{-1}$, respectively) compared to Sy-KO_Kob-KO which showed the lowest A_{sat} (5.60 ± 0.3 μmol $m^{-2}s^{-1}$), while Sy-KO_Kob-WT showed an intermediate A_{sat} level (6.39 ± 0.56 μmol $m^{-2}s^{-1}$) ($P < 0.001$). Stomatal conductance (g_s) followed a similar trend ($P < 0.001$) (Fig. 4b), with Sy-WT_Kob-WT showing the highest value (0.115 ± 0.008 mol $m^{-2}s^{-1}$) and Sy-KO_Kob-KO the lowest (0.051 ± 0.003 mol $m^{-2}s^{-1}$). The mixed combinations displayed intermediate values (Sy-KO_Kob-WT: 0.070 ± 0.004 mol $m^{-2}s^{-1}$ and Sy-WT_Kob-KO: 0.098 ± 0.006 mol $m^{-2}s^{-1}$). As expected, an opposite trend was recorded for intrinsic water use efficiency ($_i$*WUE*) with a progressive increase from Sy-WT_Kob-WT to Sy-KO_Kob-KO plants, suggesting a rootstock-to-scion influence on gas exchange dynamics (Fig. 4c). Consistent with photosynthetic data, Syrah WT plants exhibited a significantly higher total leaf area and biomass (fresh and dry weight of leaves and stem and petiole) compared to Syrah KO (Fig. S7).

To explore possible changes in water transport capacity due to *VviEPFL9*-2 mutation, we analyzed xylem vessel characteristics in the stem of scion and rootstock from each of the four groups of grafted plants (Fig. 5). The number of xylem vessels per section area varied significantly across groups: the Sy-KO_Kob-KO showed the highest density of xylem vessels in the stem (mean value of 129 ± 32.1 vessels/mm^2). In contrast Kob-WT either with Sy-WT or Sy-KO as scion, had the lowest (mean values 73 ± 9.6 and 60 ± 8.5 vessels/mm^2 respectively) (Fig. 5a). In contrast, the xylem vessel area (mm^2) was significantly smaller in the Sy-KO_Kob-KO, showing an average vessel area of 8,93 × 10^{-4} mm^2 while Sy-WT_Kob-WT had the highest of 14.5 × 10^{-4} mm^2 and the combination Sy-WT_Kob-KO and Sy-WT_Kob-WT showed intermediate values (Fig. 5b). Moreover, as shown in Fig. 5c, Sy-WT_Kob-WT plants exhibited the highest theoretical hydraulic conductivity ($kg{\cdot}m^{-1}{\cdot}s^{-1}{\cdot}MPa^{-1}$), compared to Syr-KO_Kob-KO plants ($P < 0.01$). Additionally, Sy-WT_Kob-WT plants developed a significant larger stem cross-sectional area (mm^2) compared to Syr_KO–Kob_KO plants ($P < 0.001$), while mixed combination showed intermediate values (Fig. 5d). These findings suggest that the loss-of-function mutation of *VviEPFL9*-2, which has been previously associated with decreased stomatal density (Shahbaz et al., 2025) and modified root system

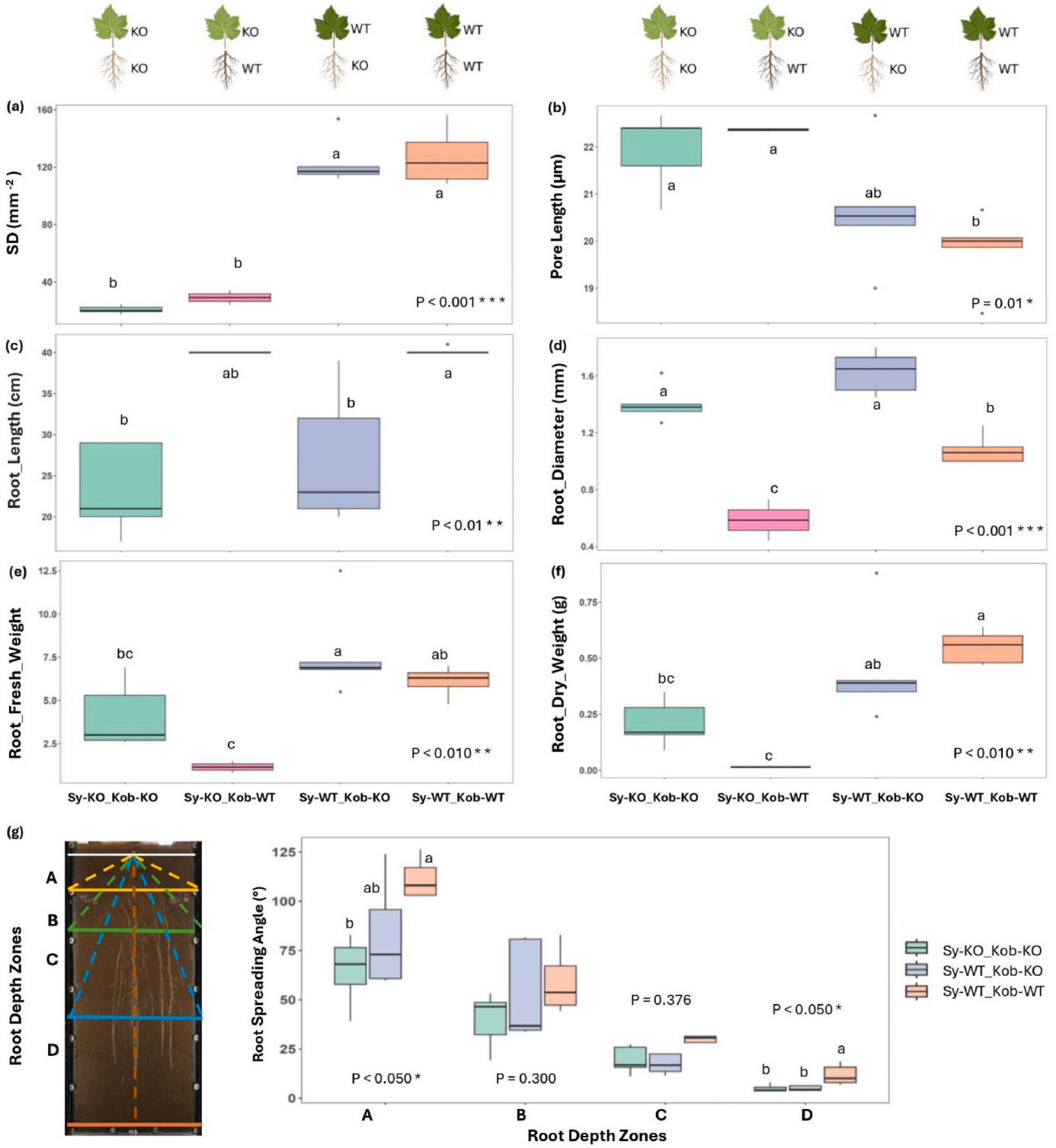


Fig. 3. Phenotyping of above (leaf) and below ground (root) traits in grafted plants grown in rhizo**trons. (a)** Stomatal density (SD mm^{-2}) and **(b)** stomatal pore length (µm) measured in mature leaves (the 5th from the apex) of the four groups of grafted plants: Sy-KO_Kob-KO, Sy-KO_Kob-WT, Sy-WT_Kob-KO and Sy-WT_Kob-WT. **(c)** Root length (cm) and **(e)** root diameter (mm) of the four groups of grafted plants measured at day 30 of the phenotyping period. **(d)** Root fresh weight and **(f)** root dry weight of the four groups of grafted plants. (**g**) On the left, representative rhizotron image illustrating root system architecture visualized in rhizotrons and divided into four depth zones (A–D) used for quantification of root spreading angle. On the right, root spreading angle (°) across depth zones (A–D) for three groups of grafted plants. Significant differences ($P < 0.05$) are denoted by different letters, according to ANOVA and subsequent post-hoc analysis. The number of biological replicates (n) for each group was 5 except for Sy-KO_Kob-WT (n = 2, and in **(g)** not analyzed).

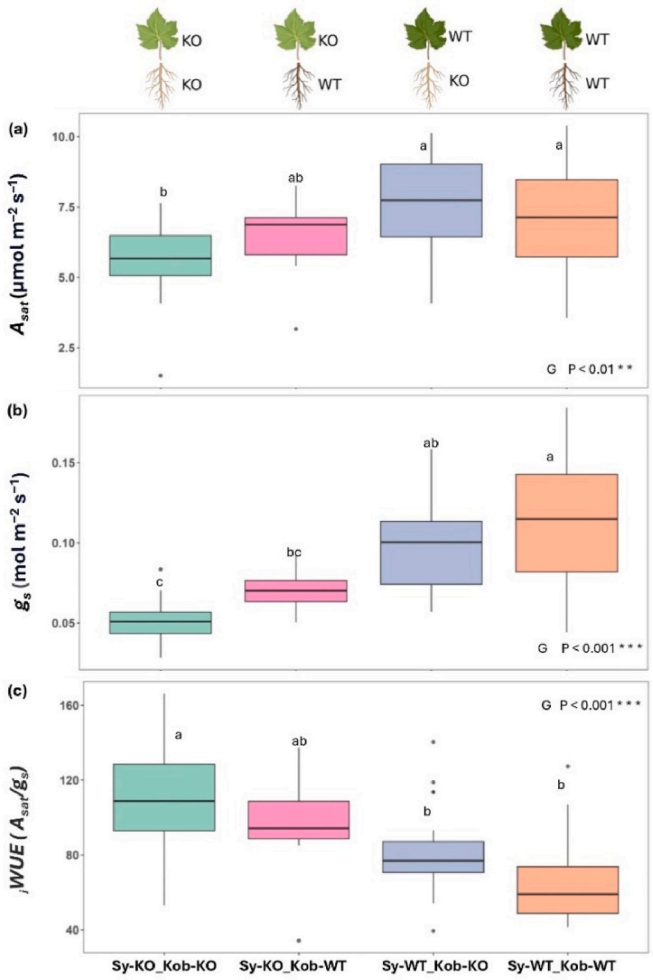


Fig. 4. Photosynthetic traits in grafted plants. (a) CO_2 assimilation rate at saturating light (A_{sat}), **(b)** stomatal conductance (g_s), and **(c)** intrinsic water-use efficiency ($_iWUE$). Statistical significance was determined by one-way ANOVA followed by Tukey's post-hoc test ($P < 0.05$). The number of biological replicates (n) for each group was 5 except for Sy-KO_Kob-WT (n = 2).

architecture (Fig. 2c,d,e), also affects stem vascular anatomy by increasing xylem vessels density and decreasing the xylem vessel area.

3.5. *EPFL9-2 knock-out activates specific metabolic pathways in grapevine roots*

To get insight about the metabolic pathways modulated by the *VviEPFL9-2* loss-of-function mutation, a RNAseq analysis of roots of edited rootstock was carried out. We compared the lists of the DEG (Differentially Expressed Genes) in the two comparisons: (i) Kob-*epfl9*-2b vs Kob-WT and (ii) Kob-*epfl9*-2a vs Kob-WT; for each pair-wise comparison, genes with an FDR-adjusted p-values below 0.05 and a fold change above 2 were considered differentially expressed. According to two-dimensional RRHO heatmap shown in Fig. S8, it appears that the majority of DEGs were shared by the two edited lines. The RRHO heatmap shows that the most intense enrichment occurred in the upper-right and lower-left quadrants, which correspond, respectively, to genes that are strongly up-regulated in both lines and strongly down-regulated in both lines. The negligible signal in the discordant quadrants (upper-left and lower-right) confirmed that the transcriptional modulation induced by *EPFL9-2* knock-out is consistent in the two independent edited lines. By exploring the transcriptomic data of genes related to major plant metabolites, a significant over representation of the genes belonging to the lignin biosynthetic pathway was found in the edited lines (Fig. 6a).

Several genes encoding different enzymes involved in many steps of lignin biosynthesis were found to be up-regulated in the edited lines: 6 genes encoding phenylalanine ammonia-lyase (PAL), the first enzyme of the phenylpropanoid pathway which is involved in the deamination of phenylalanine and leads to cinnamic acid; 1 gene encoding quinate/shikimate p-hydroxylcinnamoyltransferase (HCT); 6 genes encoding cinnamoyl-CoA reductase (CCR); 4 genes encoding cinnamyl alcohol dehydrogenase (CAD); and 7 laccase genes. The PAL enzyme is also shared by a pathway for the biosynthesis of salicylic acid (SA) although the main pathway for SA production is a different one based on chorismate. Interestingly, the isochorismate synthase gene, which belongs to the main route for SA production, is also overexpressed in the edited lines, as is a NPR1 gene, a putative receptor of SA which is essential for inducing systemic acquired resistance (Liu et al., 2020). Moreover, the transcripts of genes involved in SA catabolism (DLO and DMR6) are significantly increased in the edited lines compared to WT. These results are further supported by biochemical analysis of phytohormones in edited and WT 'Kober 5BB' plants under water stress or well water conditions. As shown in Fig. 6b, SA is slightly higher in edited lines compared to WT in both WW and WS conditions, although not significantly. However, the concentrations of the products of SA catabolism, 2,5-Dihydroxybenzoic Acid (also named Gentisic Acid) and 2,3-Dihydroxybenzoic Acid were significantly higher in the edited lines compared to WT, regardless of the water regime (WW or WS) (2,5 DHBA: Kob_WT 3.46 ± 0.43, Kob_*epfl9*-2a 6.8 ± 1.04, Kob_*epfl9*-2b 7.93 ± 1.72; 2,3 DHBA: Kob_WT 23.16 ± 6.37, Kob_*epfl9*-2a 31.33 ± 3.83, Kob_*epfl9*-2b 35.99 ± 6.87) (Fig. 6b).

Furthermore, many members of the NAC family of transcription factors were upregulated in the edited lines compared to WT (Fig. 6a) as well as a huge group of glutathione-S-transferases genes. Finally, among the significant DEG families, it is worth mentioning many CASP-like protein coding genes (Fig. 6a). Moreover, although the genes involved in auxin biosynthesis and transport are not significantly modulated overall in the edited lines, some auxin-responsive genes were found to be down-regulated in mutants compared to wild-type (WT) plants (Table S2). This finding is consistent with biochemical data indicating that the concentration of indole-3-acetic acid (IAA), the main biologically active auxin in plants, was lower in roots of edited lines compared to WT roots (Fig. 6b).

To corroborate the transcriptomic data, the components of lignin, suberin and cutin were visualized in the roots of in vitro grown Kober WT and *VviEPPFL9*-2 edited lines (Fig. 6c). As expected, we observed Auramine-O staining in the protoxylem (px) and Casparian strips (cs) in the differentiated root zone of WT, while no staining was observed in the root meristem zone. By contrast, the root tips of the *VviEPPFL9*-2 edited lines accumulate Auramine-O staining in the root cap tissue of the root meristem.

This suggests that lignin or acidic and unsaturated wax or cutin are accumulating in the root cap of the mutant lines. The direct red 23 dye, a general marker for the cell wall, did not penetrate the roots in the mutant lines, possibly suggesting that an altered cell wall composition may impede efficient dye penetration into root tissues.

4. Discussion

While a substantial body of evidence from model plants (Doheny-Adams et al., 2012), cereals (Karavolias et al., 2023) and fruit tree (Clemens et al., 2022; Shahbaz et al., 2025) links *EPFL9* loss-of-function to reduced stomatal density and altered plant water relations, the role of this gene in root tissues remains largely unexplored. In our study, the root architecture of *epfl9*-2 'Kober 5BB' mutants was found to be substantially altered compared to wild-type (WT) plants (Fig. 1; Supplementary Fig. S3). The mutant phenotype, characterized by shorter primary root length, reduced branching, narrower geotropic angle, and larger mean diameter compared to WT, bears striking similarities to those previously identified by Zhou et al. (2018) as associated

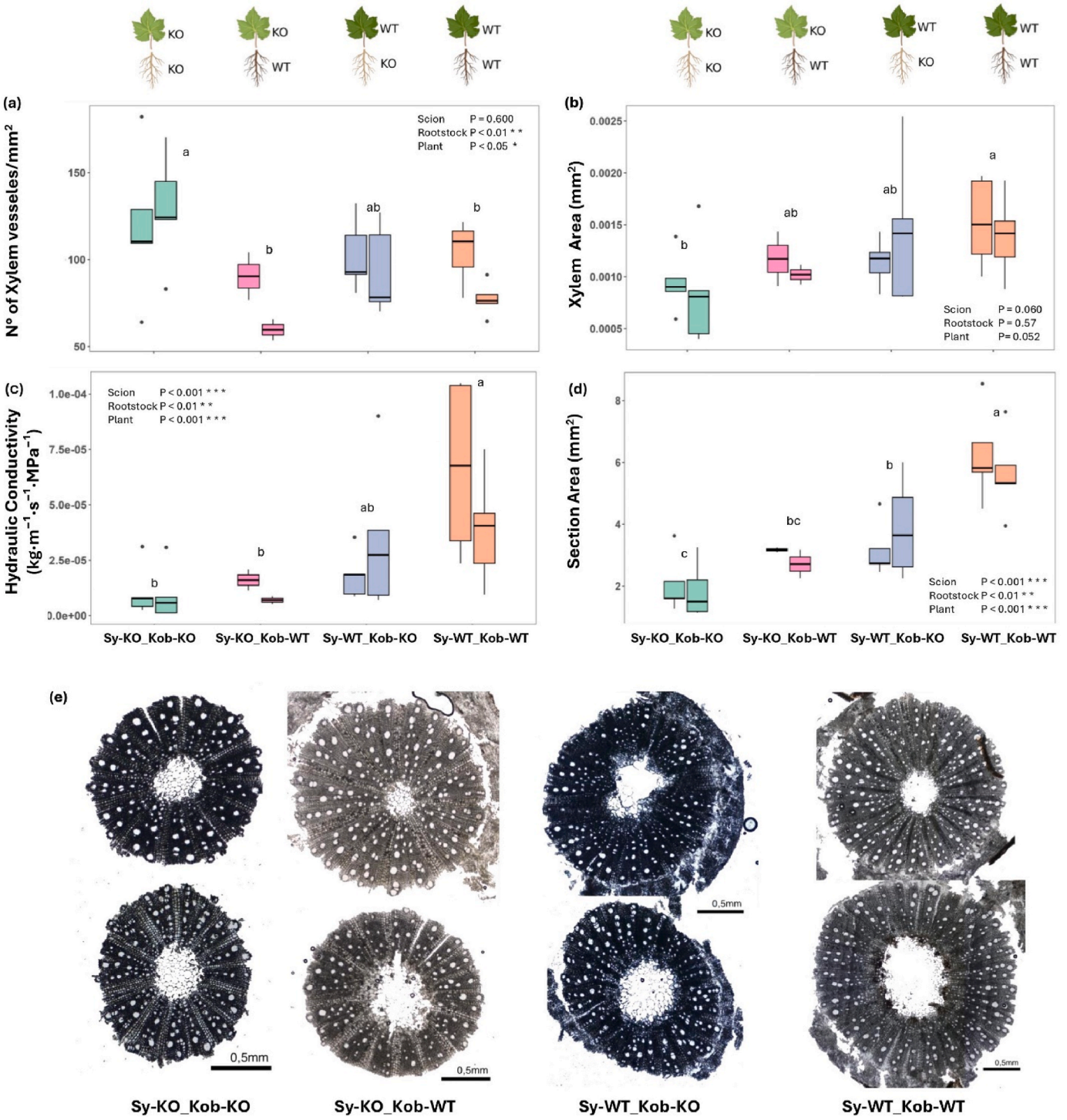


Fig. 5. Anatomical characterization of xylem vessels in grafted p**lants. (a)** Xylem vessel density (number of vessels per mm^2); (**b**) mean xylem vessel area (mm^2); (**c**) theoretical hydraulic conductivity; (**d**) stem cross-sectional area (mm^2). In panels (a–d), paired boxplots represent the scion (left box) and rootstock (right box) for each grafting combination. Data are presented as boxplots (n = 5, except for Sy-KO_Kob-WT where n = 2). Different letters indicate statistically significant differences according to Two-Way ANOVA followed by Tukey's *post-hoc* test ($P < 0.05$). (**e**) Representative light microscopy images of stem cross-sections for the four grafting combinations: Sy-KO_Kob-KO, Sy-KO_Kob-WT, Sy-WT_Kob-KO and Sy-WT_Kob-WT. For each group, the top image corresponds to the scion stem, and the bottom image to the rootstock stem. Scale bars: 0.5 mm.

with drought. These morphological alterations mirror ABA-mediated responses to water deficit. Key mechanisms include the inhibition of root elongation via SnRK2.2 and SnRK2.3 activation (Fujii et al., 2007), the repression of lateral root formation (xerobranching; Orman-Ligeza et al., 2018), and the modulation of hydrotropism (Dietrich et al., 2017). Additionally, ABA signaling activates SWEET sucrose transporters via SnRK2.2, enhancing sugar allocation to roots and increasing the root-to-shoot biomass ratio (Chen et al., 2022). Moreover, it has been reported in *Arabidopsis* that EPF factors and their ERECTA receptor may regulate root cortex proliferation during an oxidative stress, increasing the cortex layers to protect the inner vessels, thus influencing plant tolerance to drought (Cui et al., 2014; Qin et al., 2011).

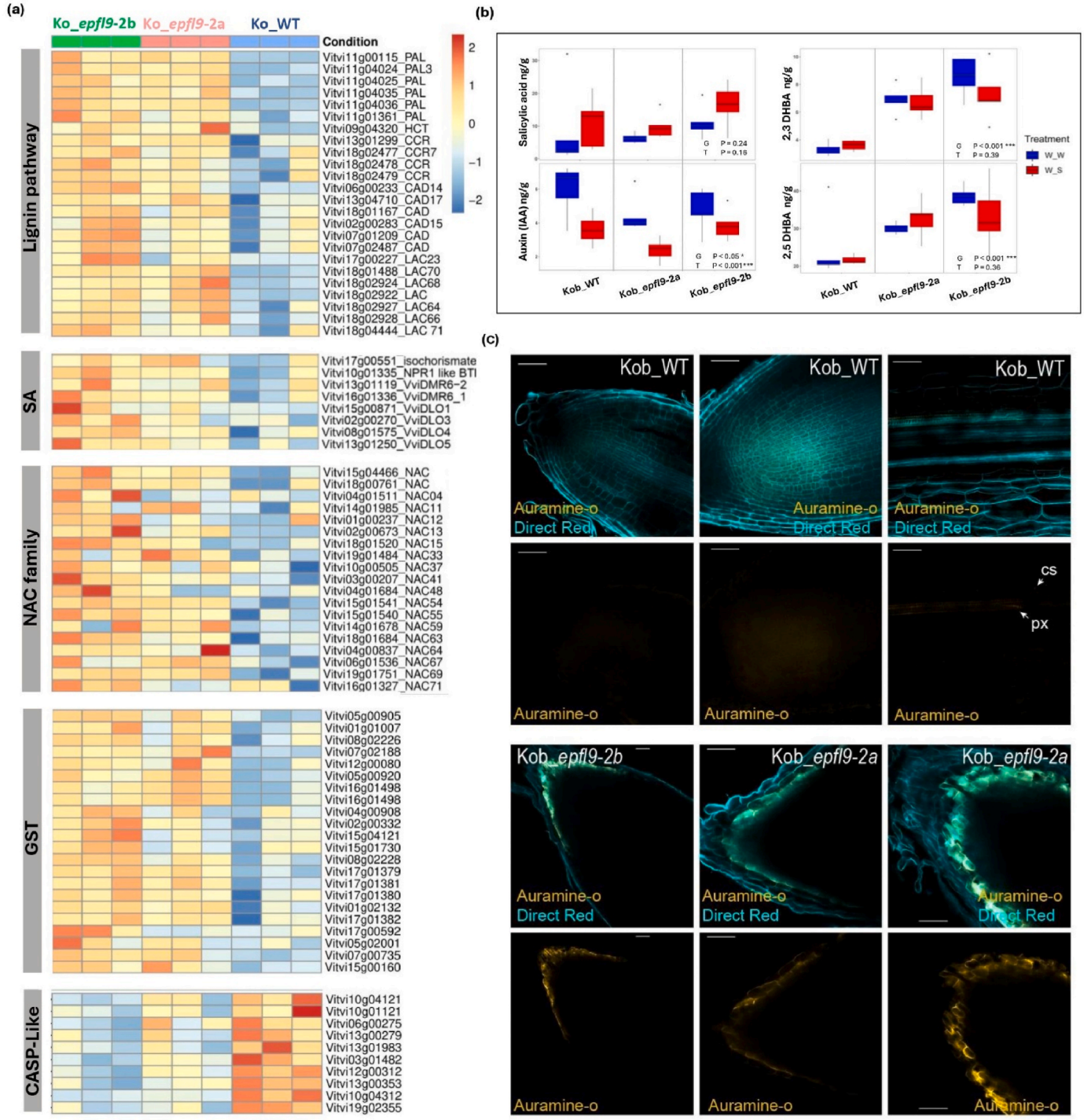


Fig. 6. Metabolic pathways modulated in roots of *epfl9-2* mutants and WT rootstocks. (a) The heatmap shows the expression patterns of genes associated with lignin biosynthesis, salicylic acid (SA) metabolism, NAC transcription factors, glutathione S-transferases (GST), and CASP-like proteins in *epfl9*-2 knockout mutants (Kob_*epfl9*-2a, Kob_*epfl9*-2b) and wild-type (Kob_WT) plants. The number of biological replicates (n) for each line and WT was 3. The expression values are represented as log2 fold-change, with red indicating upregulation and blue indicating downregulation. Genes within each pathway are labeled with their corresponding gene IDs. (**b**) Metabolite concentration of salicylic acid, (b) 2,3-dihydroxybenzoic acid (2,3-DHBA), and (c) 2,5-dihydroxybenzoic acid (2,5-DHBA) and auxin (IAA) expressed in ng/g of root fresh weight. Statistical significance was determined by one-way ANOVA followed by Tukey's post-hoc test ($P < 0.05$). The number of biological replicates (n) for each line and WT was 5. (**c**) Representative confocal images of root tips from 45-day old in-vitro grown plants that were sequentially stained with Auramine-O (targeting lignin, suberin, cutin) and Direct Red (targeting cellulose, used as a general cell wall stain); Upper panel shows the composite images from both channels and lower part show only the Auramine-O channel. Scale Bar are 50 μm. cs: Casparian strip, px: protoxylem.

In this regard, Klein et al. (2020) conducted a study on 400 maize genotypes, categorized as either best or worst performer under water stress. The study concluded that increased root aerenchyma content and larger cortical cells are favorable traits for drought tolerance. In maize, the genetic regulation of the root cortical aerenchyma has been associated to the transcription factor bHLH121 (Schneider et al., 2023).

Regarding the geotropic angle, generally, the capacity for deep rooting is associated with drought tolerance, whereas a shallow root

system provides limited drought adaptation (Lynch, 2013; Kalra et al., 2024). To this regard, the analysis of a panel of rootstocks (Fig. S1) supports the correlation between a high *EPFL9*-2 expression and a shallow root habitus. Our results showed that genotypes belonging to the *Vitis berlandieri* x *Vitis riparia* group, such as 'SO4' and 'Kober 5BB', expressed more *VviEPFL9*-2 under in vitro conditions compared with other groups, such as *Vitis berlandieri* x *Vitis rupestris* group (which includes '1103 Paulsen' and '110 Richter'). According to the PlantGrape website (https://www.plantgrape.fr/en), 'SO4' has a shallow root profile with an expanded geotropic angle and is suited to moist soils, while '1103 Paulsen' and '110 Richter' have a deep root system with a narrow geotropic angle and are more adapted to dry conditions. 'Kober 5BB', which express *VviEPFL9-2* at intermediate level between 'SO4' and '110 Richter' exhibits an in-between phenotype and behavior.

To confirm whether *VviEPFL9*-2 plays a specific role in determining the root system architecture in grapevine and to exclude the possibility that the *epfl9*-2 root phenotype is solely due to the indirect physiological effects of reduced stomatal density (SD) (Hepworth et al., 2016), we evaluated *epfl9*-2 edited rootstocks grafted with edited (lower SD) or WT (not altered SD) 'Syrah' scions (Fig. 3). The persistence of the mutant root phenotype, regardless of the scion genotype, supports the hypothesis that *VviEPFL9*-2 contributes to the regulation of root morphogenesis and may act locally in the root. Our grafting experiment also provided insights into possible rootstock-to-scion effects. In fact, it was interesting to observe the intermediate gas-exchange behavior of the grafted plants with a mixed combination of KO/WT. Notably, KO rootstocks reduced stomatal conductance (g_s) in WT scions, whereas WT rootstocks increased g_s in KO scions (Fig. 4). Data on xylem conductivity also supports the hypothesis that the KO rootstock can affect WT scion traits, albeit these data should be interpreted with caution, as this is a theoretical estimate rather than a direct measurement of water flow (Fig. 5). High xylem vessel density and reduced xylem vessel area, associated with the KO genotype, are favorable traits for avoiding water stress damage such as embolism and vessels cavitation (Holste et al., 2006; Tombesi et al., 2010). Since the drought effect on xylem vessels seems to be variety-specific (Palliotti et al., 2014), this trait has been often considered crucial in defining stress-tolerant/-sensitive genotypes.

The transcriptomic and hormonal analysis of edited and WT roots shed light on the molecular mechanisms responsible for the root phenotype in *epfl9*-2 mutants. The most significantly differentially expressed pathways and gene families between WT and edited lines were the lignin and SA pathways, NAC transcription factor, glutathione S-transferases and CASP-like gene families (Fig. 6a). Lignin is a polymer that is embedded in the secondary cell walls (Choi et al., 2023; Cesarino, 2019). At the root level it is mainly present in xylem vascular tissues and fibers (Barros et al., 2015) and in the Casparian strips surrounding root endodermal cells (Naseer et al., 2012) and its increased deposition has been associated with drought (Yamaguchi et al., 2010; Xie et al., 2024) and soil compaction stress (Zhu et al., 2025). Polymerization of monolignol units occurs via a radical reaction catalyzed by peroxidase (PRX) or laccases (LAC) in the apoplast (Blaschek and Pesquet, 2021). Different sets of LAC and PRX genes mediate lignification in specific tissues or cell types (Choi et al., 2023; Zhao et al., 2013). Interestingly, 5 out of the 6 laccases found in our study to be overexpressed in the edited lines (LAC64, LAC66, LAC68, LAC70, LAC71) belong to group 9 of the grapevine laccase family identified by Pilati et al. (2021). It is worth noting that this group contains exclusively *Vitis* sequences with no homologs in *Arabidopsis* and other species, and their function remains to be elucidated. The transcriptional regulation of lignin biosynthesis in plants is mainly regulated by NAC transcription factors (Choi et al., 2023). Interestingly, many NAC factors resulted to be up-regulated in the edited lines. In *Arabidopsis*, SECONDARY WALL-ASSOCIATED NAC DOMAIN PROTEIN 1 (SND1) has been demonstrated to regulate a large array of genes implicated in the synthesis of lignin and other secondary wall components (Zhong et al., 2006). As well, NAC SECONDARY WALL THICKENING PROMOTING FACTOR1 (NST1), a homologue of SND1, has been reported to be associated with the deposition of lignin after being induced by ABA signaling through the SnRK2s kinase complex (Liu et al., 2021).

As discussed above, lignin is also the main component of the Casparian strip, a ring-like cell wall structure in the root endodermis that blocks the passive flow of materials in vascular plants (Naseer et al., 2012). This lignin barrier is formed by membrane domain proteins (CASP, CASP1/2/3/4/5) which guide the assembly and activity of lignin biosynthetic enzymes (Roppolo et al., 2011). Many CASP and CASP-Like genes have been identified so far with a complex pattern of expression in roots (Yang et al., 2015) but their specific roles and functional mechanism is still not fully understood. According to our results, (i.e. the overexpression of numerous enzymes of the lignin pathway, the down-regulation of CASP-like genes and the increased number of xylem vessels in the stem) we speculated that lignin upregulation in the edited roots is most likely related to new xylem formation, rather than to Casparian strip. Finally, confocal microscopy (Fig. 6c) revealed a distinct accumulation of lignin, suberin, and cutin in the root cap of *epfl9*-2 edited lines. The root cap functions as a protective barrier for the root meristem and a sensory hub for soil stimuli (Arnaud et al., 2010; Ganesh et al., 2022). While the accumulation of suberin and lignin in specific root zones is a well-documented response to abiotic stress (Baxter et al., 2009; Kotula et al., 2009), the precise biochemical composition and accumulation dynamics under stress remain to be fully elucidated (Schreiber, 2010; Berhin et al., 2019; Miyazawa and Takahashi, 2020). Recently, Zhu and colleagues (2025), through high-resolution single-cell transcriptomic and histochemical analyses, demonstrated that soil compaction induces the formation of lignin and suberin barriers in rice roots that prevent radial root water loss, a mechanism triggered by ABA.

Concomitant with lignin biosynthesis, the salicylic acid (SA) pathway appeared upregulated in edited plants. This transcriptional modulation was supported by metabolic analysis (Fig. 6b), which revealed significantly higher levels of salicylate compounds in root tissues of edited lines compared to the WT. SA plays a pivotal role in shaping the structure of the root system: while low concentrations induce auxin accumulation and promote the formation of additional cortical cell layers (Pasternak et al., 2019), high concentrations generally inhibit root growth processes. Our transcriptomic data supports a hypothetical model wherein SA accumulation in *epfl9* mutant roots antagonizes auxin signaling and transport. Specifically, the down-regulation of key auxin efflux (*PIN6*, Vitvi18g01224) and influx (*LAX2*, Vitvi08g01346) carriers, together with major transcriptional regulators (*ARF5/MP*, *ARF6*) and primary response markers (*SAURs*, *Aux/IAAs*) (Table S2), suggests a disruption in polar auxin transport. This SA-auxin crosstalk hypothesis provides a plausible molecular framework explaining the altered auxin content (Fig. 6b) and the steeper root angle observed in roots of edited lines. Furthermore, the *epfl9*-2 loss-of-function modulated the expression of Glutathione S-transferases (GSTs), enzymes critical for the detoxification of Reactive Oxygen Species (ROS). Overexpression of GSTs has been previously linked to enhanced antioxidant capacity and drought tolerance (Srivastava et al., 2019).

Our results suggest that the full repression of *VviEPFL9*-2 may trigger a systemic response mimicking water stress adaptation, coordinating both shoot and root traits. This supports the existence of a genetic framework regulating the root-shoot crosstalk in water uptake (Tardieu et al., 2017). Based on these findings, a hypothetical model of the molecular mechanisms underlying these phenotypic shifts is presented in Fig. 7. Under water stress conditions, abscisic acid accumulation activates sucrose non-fermenting-related protein kinase 2 enzymes (SnRK2) (Mustilli et al., 2002; Fujii et al., 2007). These kinases mediate the ABA signaling by phosphorylating downstream targets, including the transcription factors ABF that bind to ABA-responsive elements (ABRE) in the promoters of target genes (Ng et al., 2014). Since ABA-mediated repression of *VviEPFL9*-2 has been demonstrated (Shahbaz et al.,

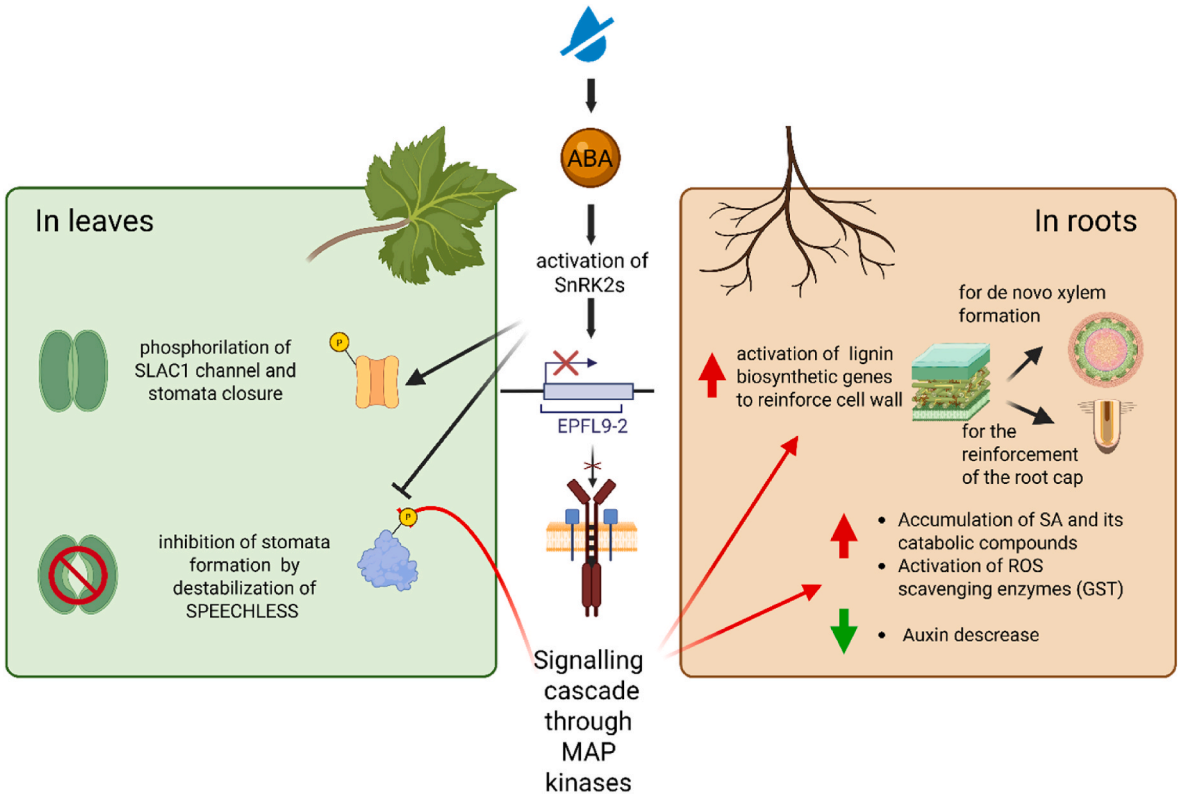


Fig. 7. Model of the molecular mechanisms upstream and downstream of VviEPFL9-2, potentially activated by wat**er stress.** ABA, whose levels increase in response to drought, activates SnRK2 kinases, which activates SLAC1 channel (Yang et al., 2022), destabilizes SPEECHLESS and mediate the ABA-dependent regulation of many genes. One such target may be *VviEPFL9*-2, which is repressed (Shahbaz et al., 2025). Without EPFL9-2, the heterodimeric receptor ERECTA-TMM constitutively activates a MAPK signaling cascade, leading to SPCH destabilization in leaf epidermal cells and, in turn, to a reduction in stomatal density and water transpiration. Furthermore, SnRK2 kinases reinforce SPCH degradation by phosphorylating specific residues. In roots, the ERECTA-TMM signaling cascade may activate lignin biosynthetic genes for de novo xylem vessel production to protect against embolisms and cavitation, and to form a barrier at the root cap level to improve tolerance to osmotic stress. Genes involved in the production of salicylic acid (SA) are also activated, as are ROS-scavenging enzymes such as glutathione S-transferases (GSTs). A decrease in auxin levels, which is consistent with the perception of stress, could be a consequence of SA accumulation. The schematic representation was generated with Biorender (https://app.biorender.com/).

2025), we postulate that these ABF factors may directly inhibit *VviEPFL9*-2 expression. While the downstream cascade leading to reduced stomatal density via MAPK inhibition is well-established (Shpak, 2013), the pathway driving root modification was unknown. Our findings identified the activation of the lignin and salicylic acid (SA) pathways as the main outcomes, likely mediated by NAC transcription factors (Liu et al., 2021). Elevated SA concentrations may reduce auxin levels, thereby reshaping root architecture (Pasternak et al., 2019). Finally, the concurrent upregulation of GST enzymes suggests that this pathway also modulates the ROS scavenging system, further enhancing stress tolerance.

To the best of our knowledge, this is the first report identifying a single gene target in grapevine, *VviEPFL9*-2, whose knockout simultaneously improves both shoot and root traits, enhancing plant adaptation to water deficit. As climate change poses a growing threat to global viticulture (van Leeuwen et al., 2024), the availability of drought-resilient genotypes (both elite varieties and rootstocks) holds significant applicative potential. Furthermore, our findings suggest that decoupling shoot and root traits by editing *VviEPFL9*-2 exclusively in the rootstock can confer systemic benefits to the entire grafted plant. This effect, mediated by rootstock-to-scion signaling, opens new avenues for improving vineyard water use efficiency while preserving the genetic identity of premium scion varieties.

Author contributions

US performed the molecular, physiological, and morphological characterization of plants, interpreted the data, and contributed to the writing of the manuscript. PV generated the edited lines and interpreted the data. SU performed confocal imaging. AZ conducted xylem vessel analysis. SP built the rhizotrons and, together with SA, contributed to data collection during the greenhouse experiments. PS and MP contributed to the analysis of transcriptomic data. PLB contributed to the xylem vessel analysis and provided rootstock plant material. DM performed metabolomic analysis. MM revised the manuscript. PS, OZ, FF, and MF interpreted the data and critically revised the manuscript. LDC conceived and designed the research, interpreted the data, and wrote the manuscript.

Declaration of competing interest

The authors declare that they have no conflicts of interest.

Acknowledgements

We thank Oscar Giovannini and Alessandra Zatelli for their essential assistance with plant management in greenhouse, Valentino Poletti for in vitro plant management, Federico Rossi and Manuel Palla for their support with qPCR analysis and greenhouse experiments. Special thanks go to Federico Pedrazzolli for his support with xylem vessel imaging. We fondly remember Claudio Moser, whose suggestions were fundamental throughout the study. This research was carried out within the framework of a PhD project co-funded by Fondazione Edmund Mach (funded by the Autonomous Province of Trento) and the Mercier Group.

Appendix A. Supplementary data

Supplementary data to this article can be found online at https://doi.org/10.1016/j.plaphy.2026.111732.

Data availability

The original contributions presented in the study are included in the article and Supplementary Material. Further inquiries can be directed to the corresponding author. Transcriptomic data are available in the NCBI database under BioProject accession number PRJNA1256299 (release date: 31 Jan 2026).

References

Arnaud, C., Bonnot, C., Desnos, T., Nussaume, L., 2010. The root cap at the forefront. C. R. Biol. 333, 335–343.

Atak, A., 2025. *Vitis* species for stress tolerance/resistance. Genet. Resour. Crop Evol. 72, 2425–2444.

Barros, J., Serk, H., Granlund, I., Pesquet, E., 2015. The cell biology of lignification in higher plants. Ann. Bot. 115, 1053–1074.

Baxter, I., Hosmani, P.S., Rus, A., Lahner, B., Borevitz, J.O., Muthukumar, B., et al., 2009. Root suberin forms an extracellular barrier that affects water relations and mineral nutrition in *Arabidopsis*. PLoS Genet. 5, e1000492.

Bemis, S.M., Lee, J.S., Shpak, E.D., Torii, K.U., 2013. Regulation of floral patterning and organ identity by *Arabidopsis* ERECTA-family receptor kinase genes. J. Exp. Bot. 64, 5323–5333.

Bergmann, D.C., Lukowitz, W., Somerville, C.R., 2004. Stomatal development and pattern controlled by a MAPKK kinase. Science 304, 1494–1497.

Berhin, A., de Bellis, D., Franke, R.B., Buono, R.A., Nowack, M.K., Nawrath, C., 2019. The root cap cuticle: a cell wall structure for seedling establishment and lateral root formation. Cell 176, 1367–1378.

Blaschek, L., Pesquet, E., 2021. Phenoloxidases in plants—how structural diversity enables functional specificity. Front. Plant Sci. 12, 754601.

Cahill, K.M., Huo, Z., Tseng, G.C., Logan, R.W., Seney, M.L., 2018. Improved identification of concordant and discordant gene expression signatures using an updated rank-rank hypergeometric overlap approach. Sci. Rep. 8, 9588.

Cesarino, I., 2019. Structural features and regulation of lignin deposited upon biotic and abiotic stresses. Curr. Opin. Biotechnol. 56, 209–214.

Chen, Q., Hu, T., Li, X., Song, C.-P., Zhu, J.-K., Chen, L., Zhao, Y., 2022. Phosphorylation of SWEET sucrose transporters regulates plant root:shoot ratio under drought. Nat. Plants 8, 68–77.

Chen, S., Zhou, Y., Chen, Y., Gu, J., 2018. Fastp: an ultra-fast all-in-one FASTQ preprocessor. Bioinformatics 34, i884–i890.

Choi, J., Makarem, M., Lee, C., Lee, J., Kiemle, S., Cosgrove, D.J., Kim, S.H., 2023. Tissue-specific directionality of cellulose synthase complex movement inferred from cellulose microfibril polarity in secondary cell walls of *Arabidopsis*. Sci. Rep. 13, 22007.

Clemens, M., Faralli, M., Lagreze, J., Bontempo, L., Piazza, S., Varotto, C., Malnoy, M., Oechel, W., Rizzoli, A., Dalla Costa, L., 2022. *VvEPFL9-1* knock-out via CRISPR/Cas9 reduces stomatal density in grapevine. Front. Plant Sci. 13, 878001.

Cui, H., Kong, D., Wei, P., Hao, Y., Torii, K.U., Lee, J.S., Li, J., 2014. SPINDLY, ERECTA, and its ligand STOMAGEN have a role in redox-mediated cortex proliferation in the *Arabidopsis* root. Mol. Plant 7, 1727–1739.

Dalla Costa, L., Piazza, S., Campa, M., Flachowsky, H., Hanke, M.-V., Malnoy, M., 2016. Efficient heat-shock removal of the selectable marker gene in genetically modified grapevine. Plant Cell Tissue Organ Cult. 124, 471–481.

Dalla Costa, L., Vinciguerra, D., Giacomelli, L., Salvagnin, U., Piazza, S., Spinella, K., Malnoy, M., Moser, C., Marchesi, U., 2021. Integrated approach for the molecular characterization of edited plants obtained via *Agrobacterium tumefaciens*-mediated gene transfer. Eur. Food Res. Technol. 248, 289–299.

Dietrich, D., Pang, L., Kobayashi, A., Fozard, J.A., Boudolf, V., Bhosale, R., et al., 2017. Root hydrotropism is controlled via a cortex-specific growth mechanism. Nat. Plants 3, 1–8.

Doheny-Adams, T., Hunt, L., Franks, P.J., Beerling, D.J., Gray, J.E., 2012. Genetic manipulation of stomatal density influences stomatal size, plant growth and tolerance to restricted water supply across a growth carbon dioxide gradient. Phil. Trans. Biol. Sci. 367, 547–555.

Feng, X., Liu, R., Li, C., Li, M., Wang, Y., Li, Y., 2022. Multi-level physiological and morphological adjustment of *Haloxylon ammodendron* related to groundwater drawdown in a desert ecosystem. Agric. For. Meteorol. 324, 109096.

Fromm, H., 2019. Root plasticity in the pursuit of water. Plants 8, 236.

Fujii, H., Verslues, P.E., Zhu, J.-K., 2007. Identification of two protein kinases required for abscisic acid regulation of seed germination, root growth, and gene expression in *Arabidopsis*. Plant Cell 19, 485–494.

Gambetta, G.A., Herrera, J.C., Dayer, S., Feng, Q., Hochberg, U., Castellarin, S.D., 2020. The physiology of drought stress in grapevine: towards an integrative definition of drought tolerance. J. Exp. Bot. 71, 4658–4676.

Ganesh, A., Shukla, V., Mohapatra, A., George, A.P., Bhukya, D.P.N., Das, K.K., et al., 2022. Root cap to soil interface: a driving force toward plant adaptation and development. Plant Cell Physiol. 63, 1038–1051.

Ge, S.X., Jung, D., Yao, R., 2020. ShinyGO: a graphical gene-set enrichment tool for animals and plants. Bioinformatics 36, 2628–2629.

Guha, A., Chhajed, S.S., Choudhary, S., Sunny, R., Jansen, S., Barua, D., 2018. Hydraulic anatomy affects genotypic variation in plant water use and shows differential organ specific plasticity to drought in *Sorghum bicolor*. Environ. Exp. Bot. 156, 25–37.

He, S., Du, X., Chen, Q., Yang, J., Fei, X., 2026. Differential roles of EPF-like peptides in stomatal patterning and drought tolerance via GhERECTA1-mediated signaling in cotton. Plant Stress 20, 101316.

Hepworth, C., Turner, C., Landim, M.G., Cameron, D., Gray, J.E., 2016. Balancing water uptake and loss through the coordinated regulation of stomatal and root development. PLoS One 11, e0156930.

Holste, E.K., Jerke, M.J., Matzner, S.L., 2006. Long-term acclimatization of hydraulic properties, xylem conduit size, wall strength and cavitation resistance in *Phaseolus vulgaris* in response to different environmental effects. Plant Cell Environ. 29, 836–843.

Kalra, A., Goel, S., Elias, A.A., 2024. Understanding role of roots in plant response to drought: way forward to climate-resilient crops. Plant Genome 17, e20395.

Karavolias, N.G., Patel-Tupper, D., Seong, K., Tjahjadi, M., Gueorguieva, G.-A., Tanaka, J., et al., 2023. Paralog editing tunes rice stomatal density to maintain photosynthesis and improve drought tolerance. Plant Physiol. 192, 1168–1182.

Kim, D., Paggi, J.M., Park, C., Bennett, C., Salzberg, S.L., 2019. Graph-based genome alignment and genotyping with HISAT2 and HISAT-genotype. Nat. Biotechnol. 37, 907–915.

Klein, S.P., Schneider, H.M., Perkins, A.C., Brown, K.M., Lynch, J.P., 2020. Multiple integrated root phenotypes are associated with improved drought tolerance. Plant Physiol. 183, 1011–1025.

Kooyers, N.J., 2015. The evolution of drought escape and avoidance in natural herbaceous populations. Plant Sci. 234, 155–162.

Korotkevich, G., Sukhov, V., Budin, N., Shpak, B., Artyomov, M.N., Sergushichev, A., 2021. Fast gene set enrichment analysis. bioRxiv, 060012.

Kotula, L., Ranathunge, K., Steudle, E., 2009. Apoplastic barriers effectively block oxygen permeability across outer cell layers of rice roots under deoxygenated conditions: roles of apoplastic pores and of respiration. New Phytol. 184, 909–917.

Kou, X., Han, W., Kang, J., 2022. Responses of root system architecture to water stress at multiple levels: a meta-analysis of trials under controlled conditions. Front. Plant Sci. 13, 1079323.

Kurihara, D., Mizuta, Y., Sato, Y., Higashiyama, T., 2015. ClearSee: a rapid optical clearing reagent for whole-plant fluorescence imaging. Development 142, 4168–4179.

Law, C.W., Chen, Y., Shi, W., Smyth, G.K., 2014. Voom: precision weights unlock linear model analysis tools for RNA-seq read counts. Genome Biol. 15, R29.

Leggett, R.M., Ramirez-Gonzalez, R.H., Clavijo, B., Waite, D., Davey, R.P., 2013. Sequencing quality assessment tools to enable data-driven informatics for high throughput genomics. Front. Genet. 4, 288.

Lesmes-Vesga, R.A., Cano, L.M., Ritenour, M.A., Sarkhosh, A., Chaparro, J.X., Rossi, L., 2023. Variation in the root system architecture of peach × peach × almond backcrosses. Plants 12, 1874.

Li, P., Zhao, Z., Wang, W., Wang, T., Hu, N., Wei, Y., et al., 2024. Genome-wide analyses of member identification, expression pattern, and protein–protein interaction of EPF/EPFL gene family in *Gossypium*. BMC Plant Biol. 24, 554.

Liao, Y., Smyth, G.K., Shi, W., 2014. featureCounts: an efficient general purpose program for assigning sequence reads to genomic features. Bioinformatics 30, 923–930.

Lin, G., Zhang, L., Han, Z., Yang, X., Liu, W., Li, E., et al., 2017. A receptor-like protein acts as a specificity switch for the regulation of stomatal development. Gene Dev. 31, 927–938.

Liu, C., Yu, H., Rao, X., Li, L., Dixon, R.A., 2021. Abscisic acid regulates secondary cell-wall formation and lignin deposition in *Arabidopsis thaliana* through phosphorylation of NST1. Proc. Natl. Acad. Sci. 118, e2010911118.

Liu, S., Chen, T., Li, X., Cui, J., Tian, Y., 2024. Genome-wide identification and expression analysis of EPF/EPFL gene family in *Populus trichocarpa*. Front. Genet. 15, 1360533.

Liu, Y., Sun, T., Sun, Y., Zhang, Y., Radojičić, A., Ding, Y., et al., 2020. Diverse roles of the salicylic acid receptors NPR1 and NPR3/NPR4 in plant immunity. Plant Cell 32, 4002–4016.

Lukowitz, W., Roeder, A., Parmenter, D., Somerville, C., 2004. A MAPKK kinase gene regulates extra-embryonic cell fate in *Arabidopsis*. Cell 116, 109–119.

Lynch, J.P., 2013. Steep, cheap and deep: an ideotype to optimize water and N acquisition by maize root systems. Ann. Bot. 112, 347–357.

Lynch, J.P., 2019. Root phenotypes for improved nutrient capture: an underexploited opportunity for global agriculture. New Phytol. 223, 548–564.

McCown, B.H., Lloyd, G., 1981. Woody Plant Medium WPM—A mineral nutrient formulation for microculture of woody plant species. Hortscience 16, 453-453.

Miyazawa, Y., Takahashi, H., 2020. Molecular mechanisms mediating root hydrotropism: what we have observed since the rediscovery of hydrotropism. J. Plant Res. 133, 3–14.

Mohammed, U., Caine, R.S., Atkinson, J.A., Harrison, E.L., Wells, D., Chater, C.C., et al., 2019. Rice plants overexpressing *OsEPF1* show reduced stomatal density and increased root cortical aerenchyma formation. Sci. Rep. 9, 5584.

Mori, M., Inagaki, M.N., 2012. Root development and water-uptake under water deficit stress in drought-adaptive wheat genotypes. Cereal Res. Commun. 40, 44–52.

Mustilli, A.-C., Merlot, S., Vavasseur, A., Fenzi, F., Giraudat, J., 2002. *Arabidopsis* OST1 protein kinase mediates the regulation of stomatal aperture by abscisic acid and acts upstream of reactive oxygen species production. Plant Cell 14, 3089–3099.

Naseer, S., Lee, Y., Lapierre, C., Franke, R., Nawrath, C., Geldner, N., 2012. Casparian strip diffusion barrier in *Arabidopsis* is made of a lignin polymer without suberin. Proc. Natl. Acad. Sci. 109, 10101–10106.

Ng, L.M., Melcher, K., Teh, B.T., Xu, H.E., 2014. Abscisic acid perception and signaling: structural mechanisms and applications. Acta Pharmacol. Sin. 35, 567–584.
Orman-Ligeza, B., Morris, E.C., Parizot, B., Lavigne, T., Babé, A., Ligeza, A., et al., 2018. The xerobranching response represses lateral root formation when roots are not in contact with water. Curr. Biol. 28, 3165–3173.e5.
Palliotti, A., Tombesi, S., Frioni, T., Famiani, F., Silvestroni, O., Zamboni, M., Poni, S., 2014. Morpho-structural and physiological response of container-grown Sangiovese and Montepulciano cvv. *Vitis vinifera* to re-watering after a pre-veraison limiting water deficit. Funct. Plant Biol. 41, 634–647.
Pasternak, T., Groot, E.P., Kazantsev, F.V., Teale, W., Omelyanchuk, N., Kovrizhnykh, V., et al., 2019. Salicylic acid affects root meristem patterning via auxin distribution in a concentration-dependent manner. Plant Physiol. 180, 1725–1739.
Pilati, S., Malacarne, G., Navarro-Payá, D., Tomè, G., Riscica, L., Cavecchia, V., et al., 2021. *Vitis* OneGenE: a causality-based approach to generate gene networks in *Vitis vinifera* sheds light on the laccase and dirigent gene families. Biomolecules 11, 1744.
Plaisier, S.B., Taschereau, R., Wong, J.A., Graeber, T.G., 2010. Rank-rank hypergeometric overlap: identification of statistically significant overlap between gene-expression signatures. Nucleic Acids Res. 38, e169.
Qin, F., Kodaira, K.-S., Maruyama, K., Mizoi, J., Tran, L.-S.P., Fujita, Y., et al., 2011. SPINDLY, a negative regulator of gibberellic acid signaling, is involved in the plant abiotic stress response. Plant Physiol. 157, 1900–1913.
Ritchie, M.E., Phipson, B., Wu, D., Hu, Y., Law, C.W., Shi, W., Smyth, G.K., 2015. Limma powers differential expression analyses for RNA-sequencing and microarray studies. Nucleic Acids Res. 43, e47.
Roppolo, D., De Rybel, B., Tendon, V.D., Pfister, A., Alassimone, J., Vermeer, J.E.M., et al., 2011. A novel protein family mediates Casparian strip formation in the endodermis. Nature 473, 380–383.
Schneider, C.A., Rasband, W.S., Eliceiri, K.W., 2012. NIH Image to ImageJ: 25 years of image analysis. Nat. Methods 9, 671–675.
Schneider, H.M., Lor, V.S., Zhang, X., Saengwilai, P., Hanlon, M.T., Klein, S.P., et al., 2023. Transcription factor bHLH121 regulates root cortical aerenchyma formation in maize. Proc. Natl. Acad. Sci. 120, e2219668120.
Schneider, H.M., Lynch, J.P., 2020. Should root plasticity be a crop breeding target? Front. Plant Sci. 11, 546.
Schreiber, L., 2010. Transport barriers made of cutin, suberin and associated waxes. Trends Plant Sci. 15, 546–553.
Shahbaz, U., Videau, P., Coulonnier, E., Papon, C., Navarro-Payá, D., Valenzuela, A.V., et al., 2025. Reduced stomatal density improves water-use efficiency in grapevine under climate scenarios of decreased water availability. Plant Cell Rep. 44, 195.
Shi, X., Cao, S., Wang, X., Huang, S., Wang, Y., Liu, Z., et al., 2023. The complete reference genome for grapevine *Vitis vinifera* L. genetics and breeding. Hortic. Res. 10, uhad061.
Shpak, E.D., 2013. Diverse roles of family genes in plant development. J. Integr. Plant Biol. 55, 1238–1250.
Spinella, K., Dalla Costa, L., Shahbaz, U., La Rocca, D., Ciuffa, S., Verginelli, D., Videau, P., Zekri, O., Marchesi, U., 2025. High-Resolution Melting HRM analysis for screening edited lines: a case study in *Vitis* spp. Int. J. Plant Biol. 16, 126.
Srivastava, D., Verma, G., Chauhan, A.S., Pande, V., Chakrabarty, D., 2019. Rice *Oryza sativa* L. tau class glutathione S-transferase OsGSTU30 overexpression in *Arabidopsis thaliana* modulates a regulatory network leading to heavy metal and drought stress tolerance. Metallomics 11, 375–389.
Tardieu, F., Draye, X., Javaux, M., 2017. Root water uptake and ideotypes of the root system: whole-plant controls matter. Vadose Zone J. 16 vzj2017.05.0107.
Teng, Z., Lyu, J., Chen, Y., Zhang, J., Ye, N., 2023. Effects of stress-induced ABA on root architecture development: positive and negative actions. Crop J. 11, 1072–1079.
Tombesi, S., Johnson, R.S., Day, K.R., DeJong, T.M., 2010. Relationships between xylem vessel characteristics, calculated axial hydraulic conductance and size-controlling capacity of peach rootstocks. Ann. Bot. 105, 327–331.
Tyree, M.T., Ewers, F.W., 1991. The hydraulic architecture of trees and other woody plants. New Phytol. 119, 345–360.
Uchida, N., Tasaka, M., 2013. Regulation of plant vascular stem cells by endodermis-derived EPFL-family peptide hormones and phloem-expressed ERECTA-family receptor kinases. J. Exp. Bot. 64, 5335–5343.
Uga, Y., Sugimoto, K., Ogawa, S., Rane, J., Ishitani, M., Hara, N., et al., 2013. Control of root system architecture by DEEPER ROOTING 1 increases rice yield under drought conditions. Nat. Genet. 45, 1097–1102.
Ursache, R., Andersen, T.G., Marhavý, P., Geldner, N., 2018. A protocol for combining fluorescent proteins with histological stains for diverse cell wall components. Plant J. 93, 399–412.
Vadez, V., Grondin, A., Chenu, K., Henry, A., Laplaze, L., Millet, E.J., Carminati, A., 2024. Crop traits and production under drought. Nat. Rev. Earth Environ. 5, 211–225.
van Leeuwen, C., Sgubin, G., Bois, B., Ollat, N., Swingedouw, D., Zito, S., Gambetta, G.A., 2024. Climate change impacts and adaptations of wine production. Nat. Rev. Earth Environ. 5, 258–275.
Wang, N., Bagdassarian, K.S., Doherty, R.E., Kroon, J.T., Connor, K.A., Wang, X.Y., Wang, W., Jermyn, I.H., Turner, S.R., Etchells, J.P., 2019. Organ-specific genetic interactions between paralogues of the PXY and ER receptor kinases enforce radial patterning in *Arabidopsis* vascular tissue. Development 146, dev177105.
Xia, H., Wang, Q., Chen, Z., Sun, X., Zhao, F., Zhang, D., et al., 2024. Identification and functional analysis of the EPF/EPFL gene family in maize *Zea mays* L.: implications for drought stress response. Agronomy 14, 1734.
Xie, J., Cao, B., Xu, K., 2024. Uncovering the dominant role of root lignin accumulation in silicon-induced resistance to drought in tomato. Int. J. Biol. Macromol. 259, 129075.
Yamaguchi, H., Fukuoka, H., Arao, T., Ohyama, A., Nunome, T., Miyatake, K., Negoro, S., 2010. Gene expression analysis in cadmium-stressed roots of a low cadmium-accumulating solanaceous plant, *Solanum torvum*. J. Exp. Bot. 61, 423–437.
Yang, J., Ding, C., Xu, B., Chen, C., Narsai, R., Whelan, J., et al., 2015. A Casparian strip domain-like gene, CASPL, negatively alters growth and cold tolerance. Sci. Rep. 5, 14299.
Yang, X., Lalitha, S., Zhou, Z., Urano, D., Lau, O.S., 2022. Abscisic acid regulates stomatal production by imprinting a SnRK2 kinase–mediated phosphocode on the master regulator SPEECHLESS. Sci. Adv. 8, eadd2063.
Zhao, D., de Voil, P., Sadras, V.O., Palta, J.A., Rodriguez, D., 2025. The plasticity of root traits and their effects on crop yield and yield stability. Plant Soil.
Zhao, Q., Nakashima, J., Chen, F., Yin, Y., Fu, C., Yun, J., et al., 2013. LACCASE is necessary and nonredundant with PEROXIDASE for lignin polymerization during vascular development in *Arabidopsis*. Plant Cell 25, 3976–3987.
Zhong, R., Demura, T., Ye, Z.-H., 2006. SND1, a NAC domain transcription factor, is a key regulator of secondary wall synthesis in fibers of *Arabidopsis*. Plant Cell 18, 3158–3170.
Zhou, G., Zhou, X., Nie, Y., Bai, S.H., Zhou, L., Shao, J., et al., 2018. Drought-induced changes in root biomass largely result from altered root morphological traits: evidence from a synthesis of global field trials. Plant Cell Environ. 41, 2589–2599.
Zhu, M., Hsu, C.W., Peralta Ogorek, L.L., et al., 2025. Single-cell transcriptomics reveal how root tissues adapt to soil stress. Nature 642, 721–729.

Further reading

Carlin, S., Masuero, D., Guella, G., Vrhovsek, U., Mattivi, F., 2019. Methyl salicylate glycosides in some Italian varietal wines. Molecules 24, 3260.